Institute of Electrical and Electronic Engineering
Department of Power and Control

Final Year Project Report Presented in Partial Fulfilment of
the Requirements for the Degree of

MASTER

In **Electrical and Electronic Engineering**
Option: **Control/Power**

Title:

Simulation and Implementation of single phase, single stage, grid connected photovoltaic system

Presented by:

- **AYAD Mohamed**
- **MAHBOUBI Meriem**

Supervisors:

Dr. B.Metidji

Dr. A. Kheldoun

Registration Number:..../2016

Dedication

Every challenging work needs self-efforts as well as guidance of elders especially those who were very close to my heart.

My humble effort is dedicated to:

My sweet and loving parents whose affection, love and prayers of day and night make me able to get such success and honor.

To my sister, I am really grateful to have her in my life,

To all persons I met and in my heart they took a place.

To my uncles, to the memory of my grandparents to my friends Amira and, Thamila, my inspirations and my soul mate.

Along with all hard working and respected teachers.

Thank you for your great support and continuous care...

Meriem

I dedicate this work to my family and my friends.

Mohammed

Acknowledgement

Abstract

This work describes the single-phase, single-stage, Grid-Connected Photovoltaic System (GCPV) using Hysteresis Current Control Inverter. The complete Matlab/Simulink simulation and hardware implementation of the system are performed.

To achieve reliable and efficient power generation from photovoltaic systems; perturb and observe (P&O) maximum power point tracking (MPPT) method has been used. The latter maximizes the power from the PV system under various lighting conditions. A four-MOSFET bridge inverter that takes DC power supplied by a solar panel and transforms it into a 220 volt AC power source. A Hysteresis current controller has been employed to adjust the inverter's frequency according to the grid frequency. As compared to other control methods, the proposed solution provides robust current regulation, achieves unity power factor, low total harmonic distortion (THD) and maximizes the PV power extracted from the PV generator. Simulation and experimental results are provided and commented to demonstrate the effectiveness of the design.

Table of contents

Table of contents

List of Tables

List of figures

List of figures

List of figures

Nomenclature

A	Ampere
A	ideality factor
AC	Alternating Current
ASD	Adjustable Speed Drive
°C	Degree Celsius
CDC	Direct Current link Capacitor
CdTe	Cadmium Telluride
CIS	Copper Indium Diselenide CuInSe2
CSI	Current Source Inverter
D	diode diffusion factor
DC	Direct Current
DR	Distributed Resources
Eg:	material band-gap energy (1.12 eV for Silicon)
f	Frequency
f_s	switching frequency
FACT	Flexible AC Transmission
FET	Field Effect Transistor
G	Irradiance (W/m^2).
GaAs	Gallium Arsenide
GC	Grid Connected
GCPV	Grid Connected Photovolaic
Hz	Hertz
IEEE	Institute of Electrical and Electronics Engineers
I_D	diode current
I_g	Grid current
I_P	current leak in parallel resistor
I_{ph}	photo current
I_{pv}	PV output current
I_s	saturation current
IC	Integrated circuit
IGBT	Insulated-Gate Bipolar Transistor
K	Boltzmann constant = 1.381*10^{-23}(J/K)
°K	Degree kelvin

K_I	Temperature coefficient of short-circuit current (A/°K).
MATLAB	is the easiest and most productive software environment for engineers and scientists
MOSFET	metal–oxide–semiconductor field-effect transistor
MPPT	Maximum Power Point Tracking
N_s	the number of PV cells connected in series
P	Power
P&O	Perturb and Observe
PCU	power conditioning unit
PLL	Phase Locked Loop
PV	Photovoltaic
R_s	series resistance
R_P	parallel resistance
Ref	Reference at STC
PWM	Pulse width Modulation
q	electron charge $=1.602*10^{-19}$(C)
RMS	Root Mean Square
s	seconds
Si	Silicon
SIMULINK	a block diagram environment for Model-Based Design
SPWM	Sinusoidal Pulse width Modulation
STC	Standard Test Conditions
T	Temperature (°K).
THD	Total Harmonic Distortion
TDD	Total Demand distortion
V	Volt/voltage
$V_{control}$	sinusoidal control signal
v_{dc}	DC link voltage
V_g	Grid voltage
Voc	open circuit voltage
V_T	Thermal voltage
$V_{tri.}$	Triangular waveform
VSI	Voltage Source Inverters
W	Watt

1- Introduction

Since the beginning of the Industrial Revolution, coal, crude oil and natural gas are the three forms of fossil fuels mostly used worldwide. These non-renewable sources of energy are so called because they have been formed from the organic remains of prehistoric plants and animals and have rotted away over millions of years and became solids, liquids and gasses. They will eventually run out one day. Fossil fuels must be located, excavated and transported before they can be used. These carbon-based fuels are employed to feed power plants to produce electrical energy [1]. They must be burned to produce electricity. Burning them creates unwanted by-products such carbon dioxide. These unwanted by-products pollute the environment and contribute to global warming due to the release of huge amount of greenhouse gasses into the atmosphere. To minimize this major problem, there is a need to replace these fossil fuels with an environment friendly alternative; renewable energies.

There is a wide variety of renewable energies. These energies use resources that are naturally replenished on a human timescale and will never end. The list of these resources, ordered by the amount of contribution to the production of electricity, currently includes: hydro, wind, biomass, geothermal heat and sunlight. Electricity derived from these energies is considered "green" because of the negligible negative impacts on the environment. [2]

2- Solar Energy

Among all renewable energy sources available, solar energy is the most promising source. It is free, secure, pollution-free, available all over the world, and will last forever [3, 4].

One of many ways of generating electricity from solar energy is the use of solar modules which convert sunlight into direct electricity (DC) using the photovoltaic effect. Solar panels are formed out of interconnected photovoltaic cells that are arranged in series-parallel configuration.

There are several factors that affect the efficiency, percentage of sun's energy striking the PV cell that is converted into electricity, of the solar panel. The two major ones are: (1) the PV cell temperature T and, (2) the intensity of sun rays received on the surface of the solar panel.

Although there is a continuous improvement in the PV materials to enhance PV cell efficiency, current technology delivers PV cells with an efficiency level ranging from 10 to 20%. Therefore, to satisfy the power demand, we need to rely on the dimensions of the panels and/or the irradiation intensity. Increasing the surface area of the solar panels is not a viable solution. It increases investments cost and requires more ground surface. A more feasible and economical solution however, is to maximize power extraction from the panel by using an MPPT (maximum power tracking).

3- Historical overview

The photovoltaic effect was firstly observed by a French scientist Edmund Alexander Bacquirel in 1839 [5], but it was not fully understood until the development of quantum theory of light and solid state physics by Albert Einstein in the middle of the twentieth century. Einstein explained the ability of some semiconductor materials to convert electromagnetic radiations directly into electrical current.

At the beginning, Photo voltaic cells were demonstrated by powering toys. The first conventional photovoltaic cells were produced in the late 1950s. In 1958 they found wide acceptance as part of the space program after initial success on the Vanguard I satellite. And throughout the 1960s were principally used to provide electrical power for earth-orbiting satellites.

In the 1970s, improvements in manufacturing, performance and quality of PV modules helped to reduce costs and opened up a number of opportunities for powering remote terrestrial applications, including battery charging for navigational aids, signals, telecommunications equipment and other critical, low-power needs.

In the 1980s, photovoltaic became a popular power source for consumer electronic devices, including calculators, watches, radios, lanterns and other small battery-charging applications. Following the energy crises of the 1970s, significant efforts also began to develop PV power systems for residential and commercial uses, both for stand-alone, remote power and for utility-connected applications. [6, 7]

Table 1.1 demonstrates the evolution of the share of PV modules in different market sectors [8]

Table 1.1 The evolution of the share of PV modules in different market sectors.

Year	Total MWp Worldwide	Off-Grid % Total	Grid-Connected % Total	Consumer Indoor % Total
1997	114.1	62%	34%	4%
1998	134.8	65%	32%	4%
1999	175.5	58%	39%	3%
2000	252.0	47%	51%	2%
2001	352.9	39%	59%	2%
2002	504.9	32%	67%	1%
2003	675.3	27%	72%	1%
2004	1049.3	19%	80%	1%
2005	1407.7	17%	83%	1%
2006	1984.6	14%	86%	<1%
2007	3073.0	10%	90%	<1%
2008	5491.8	6%	94%	<1%
2009	7913.3	5%	95%	<1%
2010	17402.7	<2%	98%	<1%
2011	23579.3	1%	99%	<1%
2012	26061.8	1%	99%	<1%

**It is interesting to note that since 1997 the most growing market for PV modules are the grid connected PV systems which is the subject of this project.

4-   Objectives of the project

This work addresses the simulation and the design process of a single phase, single stage, grid connected PV system with a hysteresis current controller. The controller is implemented using Arduino due and hardware ICs.

The proposed methodology is based on MATLAB/SIMULINK to model, simulate the whole system under variable climate conditions. Then, the whole system will be implemented, **figure 1.1**.
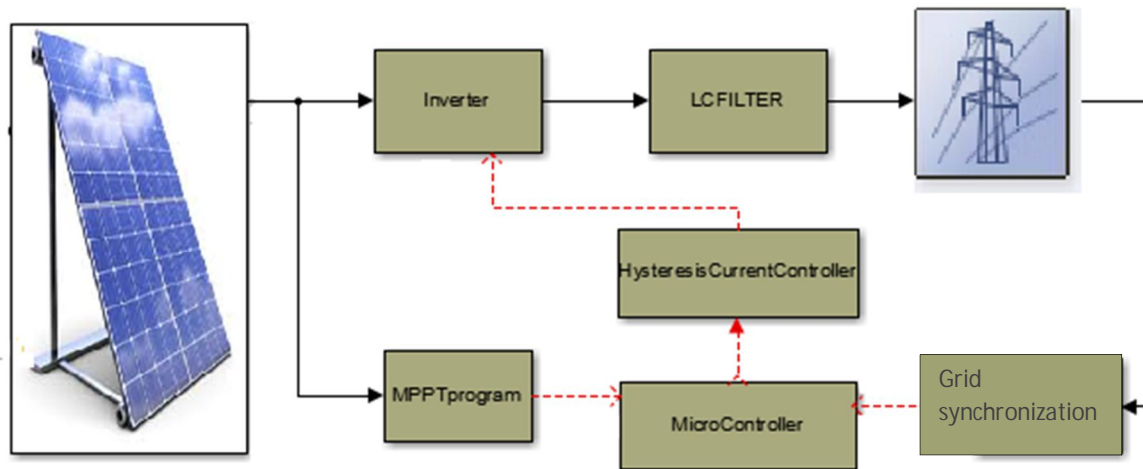
Figure 1.1 Grid connected PV system

The objectives intended to be achieved by the end of this work are:
- Model and Simulate the PV panel.
- Simulate the proposed grid connected PV system.
- Synchronize the inverter's output voltage and frequency with the national grid.
- Extract maximum power from the PV panel.
- Implement the synchronization circuit.
- Design and construct a single phase full bridge inverter.
- Implement a hysteresis current controller for the inverter's output.
- Connect the designed system to the grid.
- Evaluate the system performances.

5-   Organization of the report

This report is compiled into 6 chapters including this introduction and followed by the references used in this work. Chapter 1 introduces the problematic. It also reviews the proposed solution briefly.

In chapter 2, an overview of PV systems is presented. Chapter 3 introduces the model of PV module using MATLAB. Chapter 4 presents the simulation of the proposed grid connected PV system. It also describes each part of the system.

Chapters 5 describes in details the design and implementation of the proposed system with its both software and hardware parts. Chapter 6 concludes the project with some discussions and suggestions for future work.

Finally, the report terminates with an extensive list of references for additional information on the subject and some appendices to provide additional details on the different components used in the hardware set up, also some supporting information.

Appendix A: A detailed modeling of photovoltaic module using MATLAB [19]

Parameters of the KYOCERA KC200GT array are shown in **table A.1**.

Table A.1 KYOCERA KC200GT parameters.

I_{mp}	V_{mp}	I_{sc}	V_{oc}	R_p	R_s	P_{max}	K_I	K_v
7.61A	26.3V	8.21A	32.9V	415.405Ω	0.221Ω	200W	3.18×10⁻³A/°C	-1.23×10⁻¹V/°C

1- Photocurrent implementation I_{ph}

First, substituting equation (3.15) in equation (3.16), the photocurrent I_{ph} equation can be implemented in MATLAB/Simulink environment as shown in **figure A.1**
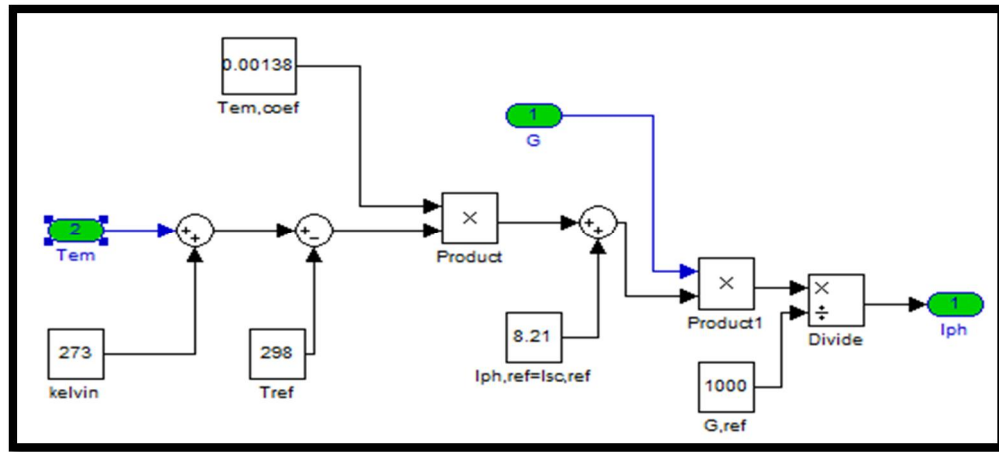
Figure A.1 I_{ph} Implementation

2- The reverse saturation current at STC implementation ($I_{s,ref}$ or $I_{0,ref}$)

Substituting equation (3.8) in equation (3.21) the current $I_{s,ref}$ can be modeled as shown in **figure A.2**.
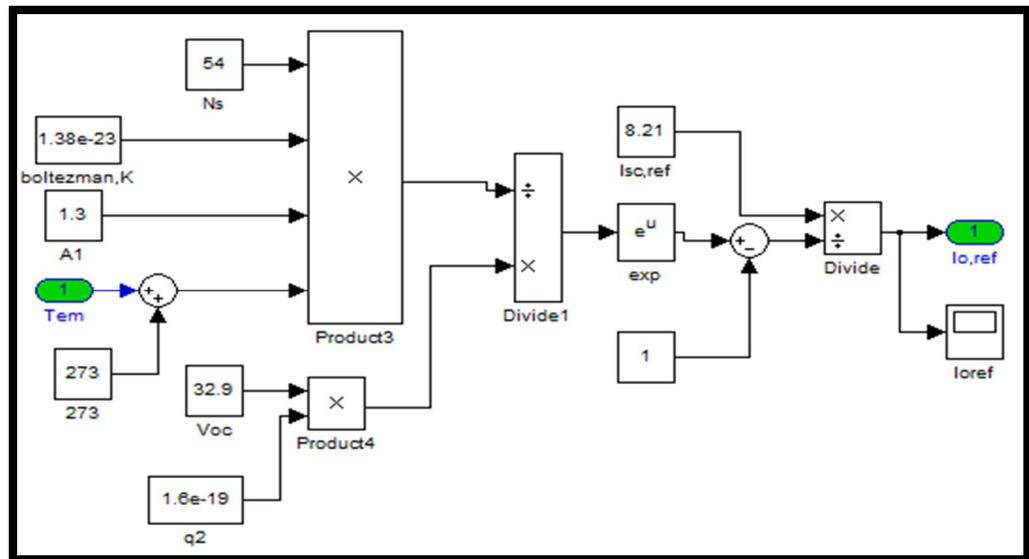
Figure A.2 $I_{0,ref}$ Implementation

3- The reverse saturation current implementation I_0

Now, after simulating $I_{0,ref}$, equation (3.23) can be implemented using Simulink in order to get I_0 as shown in the **figure A.3** :
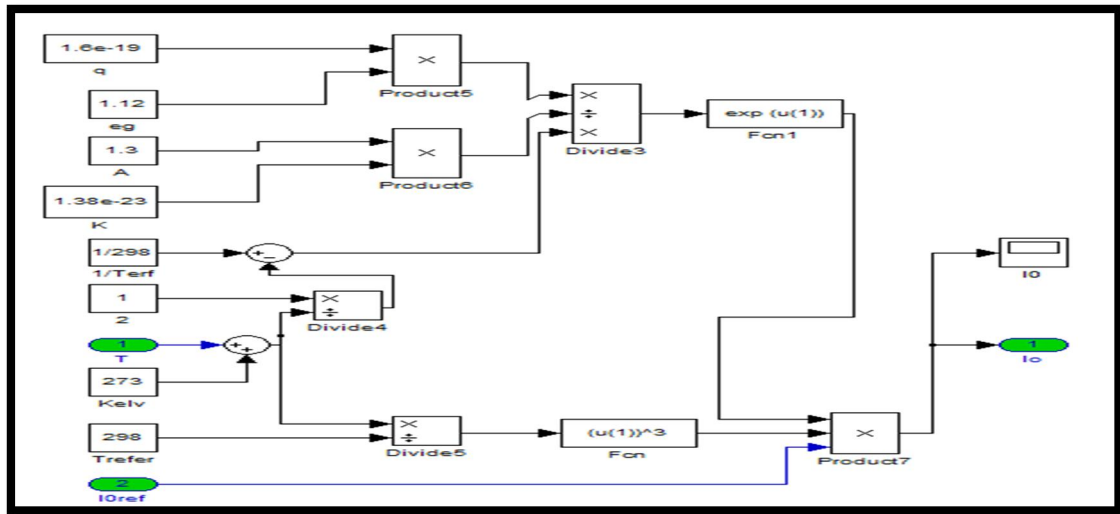
Figure A.3 I_0 Implementation

4- The panel output current implementation (I_{pv})

Now, since all the needed parameters are implemented, the equation of the output current (3.12) can be simulated, note that the term R_p has been ignored in the simulation for simplicity.
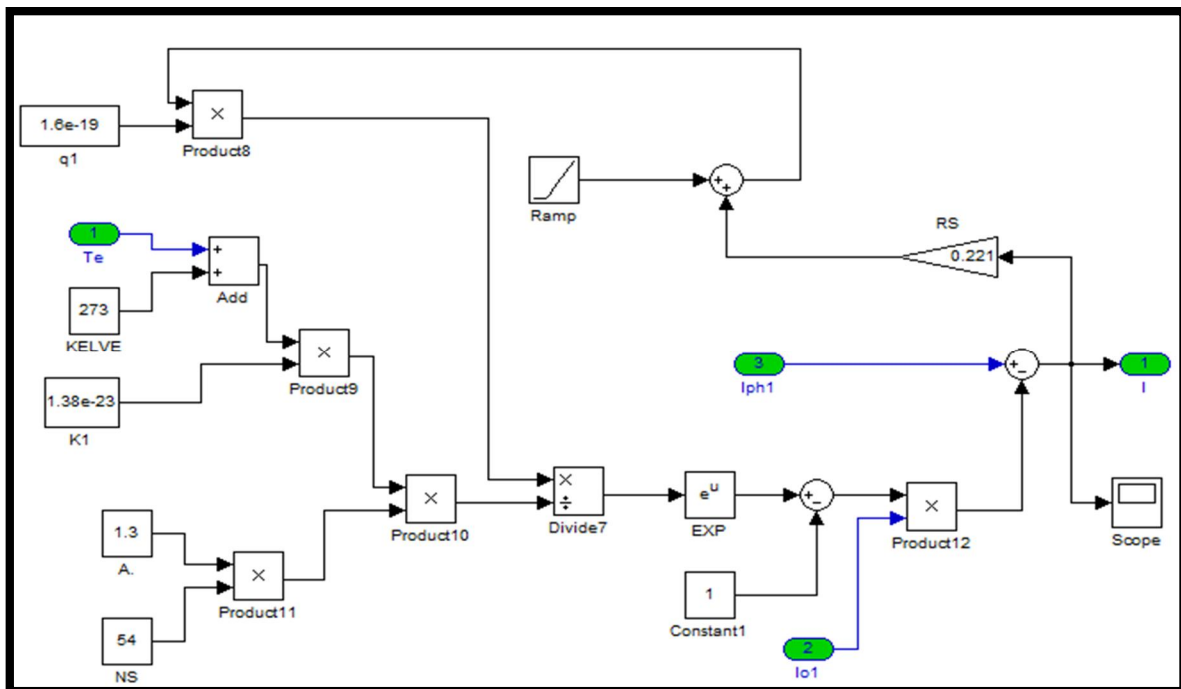
Figure A.4 Detailed model without R_p term.

The general block of this simulation is shown in **figure A.5**.
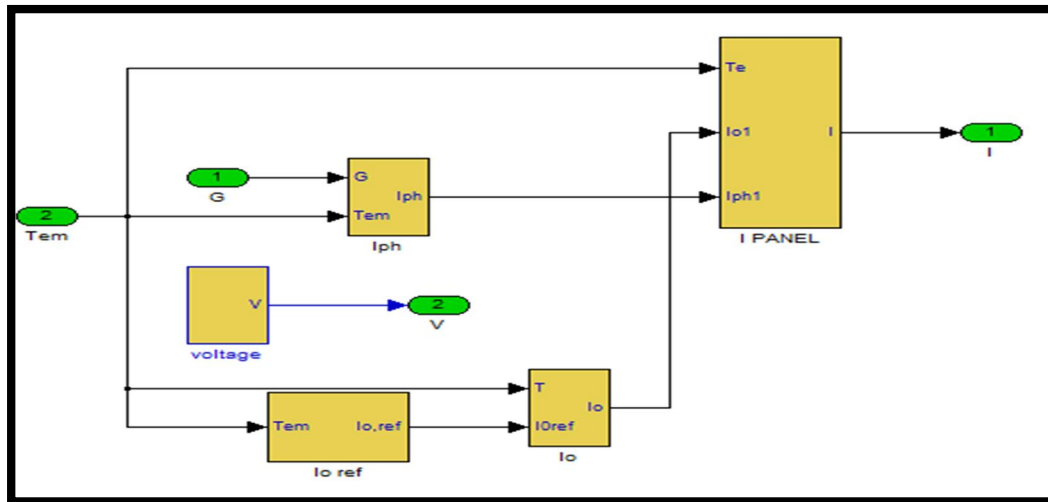
Figure. A.5 Detailed model of the PV current

❖ Note that a ramp signal is used to represent the voltage in order to observe the electrical characteristics of the PV as well as to plot I (V) and P (V) graphs later, the previous blocks can be regrouped in one block (PANEL) having two inputs which are the temperature and the irradiance and two outputs which are the current and the voltage as shown in **figure A.6**. This can help observing the effects of the temperature and the irradiance variations on the electrical characteristics of the proposed panel.

5- <u>Output curves</u>

Using scopes, it is possible to plot I (V) and P(V) for constant irradiance and temperature as shown in the following figure:
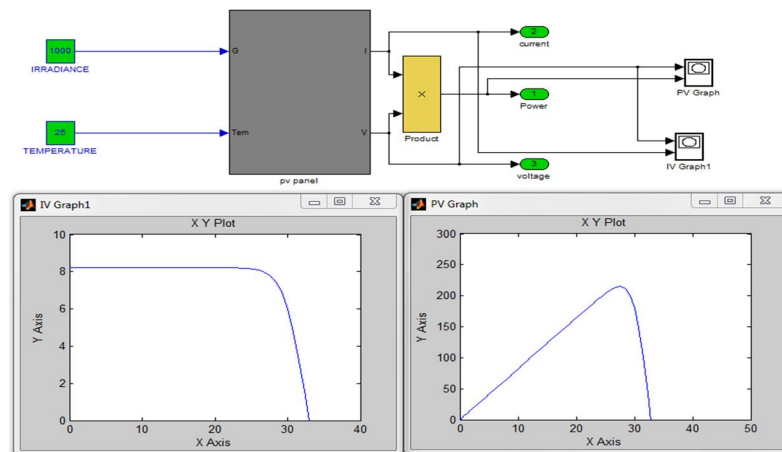
Figure. A.6 I (V) and P (V) curves

Those two graphs match the given information in the datasheet of the panel, the current is constant in a range between 0 volts and a certain voltage value, less than the open circuit voltage, where the power reach its maximum. This point is called the maximum power point MPP and a tracking system must be applied to the panel in order to keep the power maximum using some techniques known as MPPT algorithms.

- **Effect of irradiance variation on the curves:**

Using the model in **figure A.6** it is possible to observe the effect of variable irradiance on the electrical characteristics since in the reality irradiance is not constant it varies all the time depending on the time during the day, five values of irradiance have been applied to the system from 200 W/m^2 to the SCT value which is 1000W/m^2, the graph is shown in the next figure:
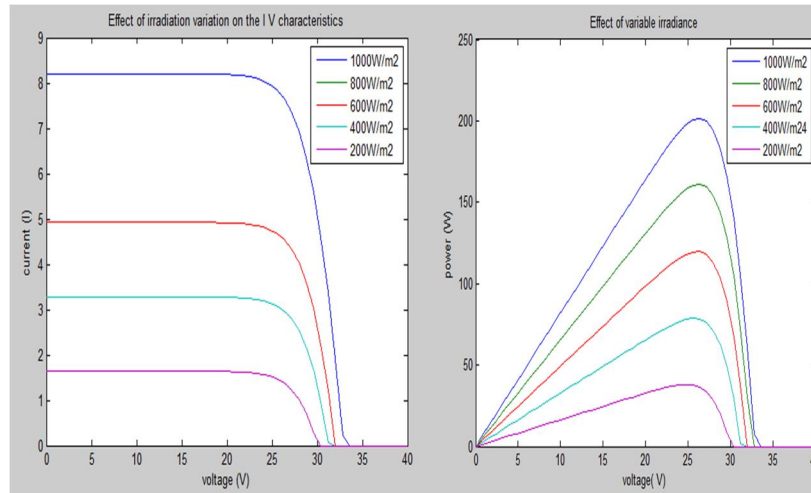
Figure. A.7 Effect of irradiance variation on the I-V and P-V characteristics

- **Effect of temperature variation on the curves**

The second input of the PV panel is the temperature and as in the case of irradiance it is never constant, it varies during the day and during the whole year, so it is very helpful in the design to know what is exactly the effect of its variation on the output ,in order to observe its effect, the system in figure (A.10) is used by applying different values of temperature to system`s input ,the variation starts from 0°C to 80°C ,the results are shown in **figure A.8**:
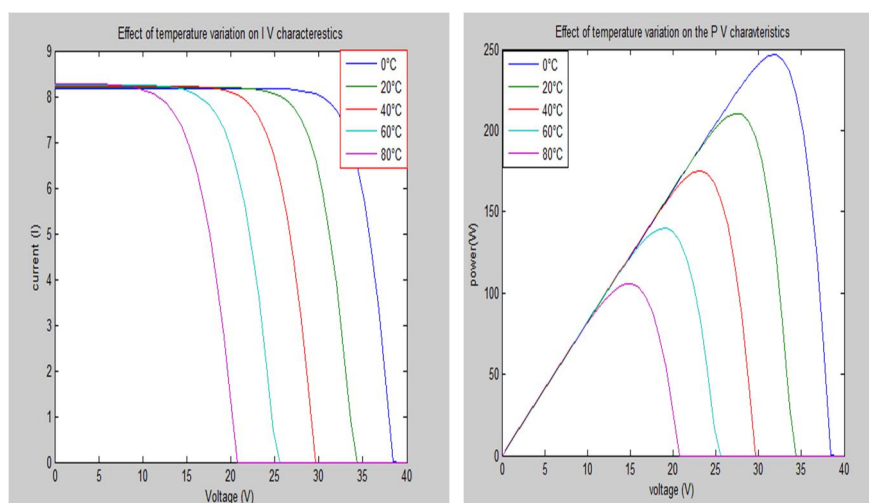
Figure A.8 Effect of temperature variation on the I-V and P-V characteristics

Appendix B: Current Transducer LA 25-P

For the electronic measurement of currents: DC, AC, pulsed..., with galvanic separation between the primary circuit and the secondary circuit.

Features

- Closed loop (compensated) current transducer using the Hall effect.
- Insulating plastic case recognized according to UL 94-V0.

Advantages

- Excellent accuracy.
- Very good linearity.
- Low temperature drift.
- Optimized response time.
- Wide frequency bandwidth.
- No insertion losses.
- High immunity to external interference.
- Current overload capability.
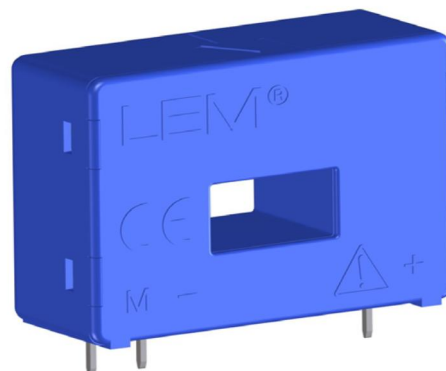
Applications

- AC variable speed drives and servo motor drives.
- Static converters for DC motor drives.
- Battery supplied applications.
- Uninterruptible Power Supplies (UPS).
- Switched Mode Power Supplies (SMPS).
- Power supplies for welding applications.

Electrical data

			$T_A = 70\ °C$		$T_A = 85\ °C$		
I_{PN}	Primary nominal rms current		25				A
I_{PM}	Primary current, measuring range		$0 .. \pm 55$				A
R_M	Measuring resistance		$R_{M\,min}$	$R_{M\,max}$	$R_{M\,min}$	$R_{M\,max}$	
	with ± 12 V	@ ± 25 A $_{max}$	10	280	60	275	Ω
		@ ± 55 A $_{max}$	10	80	60	75	Ω
	with ± 15 V	@ ± 25 A $_{max}$	50	400	135	395	Ω
		@ ± 55 A $_{max}$	50	140	135	135	Ω
I_{SN}	Secondary nominal rms current		25				mA
K_N	Conversion ratio		$1 : 1000$				
U_C	Supply voltage (± 5 %)		$\pm 12 .. 15$				V
I_C	Current consumption		$10\ (@ \pm 15\,V) + I_S$				mA

Accuracy - Dynamic performance data

				Typ	Max	
X	Accuracy @ I_{PN}, T_A = 25 °C	@ ± 15 V (± 5 %)		± 0.95		%
		@ ± 12 .. 15 V (± 5 %)		± 1.25		%
ε_L	Linearity error			< 0.15		%
I_O	Offset current @ I_P = 0, T_A = 25 °C				± 0.2	mA
I_{OM}	Magnetic offset current [1] @ I_P = 0 and specified R_M, after an overload of 3 × I_{PN}				± 0.3	mA
I_{OT}	Temperature variation of I_O	0 °C .. + 70 °C		± 0.1	± 0.5	mA
		- 25 °C .. + 85 °C		± 0.1	± 0.6	mA
t_{ra}	Reaction time			< 500		ns
t_r	Step response time to 90 % of I_{PN}			< 1		µs
di/dt	di/dt accurately followed			> 200		A/µs
BW	Frequency bandwidth (- 1 dB)			DC .. 200		kHz

General data

T_A	Ambient operating temperature		- 25 .. + 85	°C
T_S	Ambient storage temperature		- 40 .. + 90	°C
R_S	Resistance of secondary winding	@ T_A = 70 °C	80	Ω
		@ T_A = 85 °C	85	Ω
m	Mass		24	g

Insulation coordination

U_d	Rms voltage for AC insulation test, 50 Hz, 1 min		3	kV
$\hat{U}_W$	Impulse withstand voltage 1.2/50 µs		5.7	kV
			Min	
d_{Cp}	Creepage distance		5	mm
d_{Cl}	Clearance		5	mm
CTI	Comparative tracking index (group I)		600	

Safety

●This transducer must be used in limited-energy secondary circuits according to IEC 61010-1.

●This transducer must be used in electric/electronic equipment with respect to applicable standards and safety requirements in accordance with the manufacturer's operating instructions.

Appendix C: BUK555 & IR2135

In this appendix, the characteristics of the mosfet and the driver used in the full bridge inverter are given.

I. PowerMOS transistor Logic level FET BUK555-100A/B

General description

N-channel enhancement mode logic level field-effect power transistor in a plastic envelope. The device is intended for use in Switched Mode Power Supplies (SMPS), motor control, welding, DC/DC and AC/DC converters, and in automotive and general purpose switching applications.

Pin configuration

- 1 gate
- 2 drain
- 3 source
- 4 tab
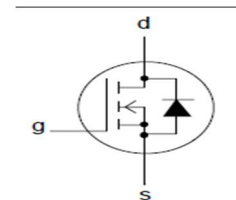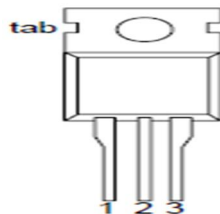
Quick reference data

SYMBOL	PARAMETER		MAX.	MAX.	UNIT
		BUK555	-100A	-100B	
V_{DS}	Drain-source voltage		100	100	V
I_D	Drain current (DC)		25	22	A
P_{tot}	Total power dissipation		125	125	W
T_j	Junction temperature		175	175	°C
$R_{DS(ON)}$	Drain-source on-state resistance; $V_{GS} = 5$ V		0.085	0.11	Ω

Limiting values

SYMBOL	PARAMETER	CONDITIONS	MIN.	MAX.		UNIT
V_{DS}	Drain-source voltage	-	-	100		V
V_{DGR}	Drain-gate voltage	$R_{GS} = 20$ kΩ	-	100		V
$\pm V_{GS}$	Gate-source voltage	-	-	15		V
$\pm V_{GSM}$	Non-repetitive gate-source voltage	$t_p \le 50$ µs	-	20		V
				-100A	-100B	
I_D	Drain current (DC)	$T_{mb} = 25$ °C	-	25	22	A
I_D	Drain current (DC)	$T_{mb} = 100$ °C	-	18	15	A
I_{DM}	Drain current (pulse peak value)	$T_{mb} = 25$ °C	-	100	88	A
P_{tot}	Total power dissipation	$T_{mb} = 25$ °C	-	125		W
T_{stg}	Storage temperature	-	-55	175		°C
T_j	Junction Temperature	-	-	175		°C

II.   PHASE BRIDGE DRIVER IR 2135

Features

- Floating channel designed for bootstrap operation
- Fully operational to +600V or+1200V
- Tolerant to negative transient voltage
- dV/dt immune
- Gate drive supply range from 10V/12V to 20V DC and
- up to 25V for transient
- Undervoltage lockout for all channels
- Over-current shut down turns off all six drivers
- Independent 3 half-bridge drivers
- Matched propagation delay for all channels
- 2.5V logic compatible
- Outputs out of phase with inputs
- All parts are also available LEAD-FREE.
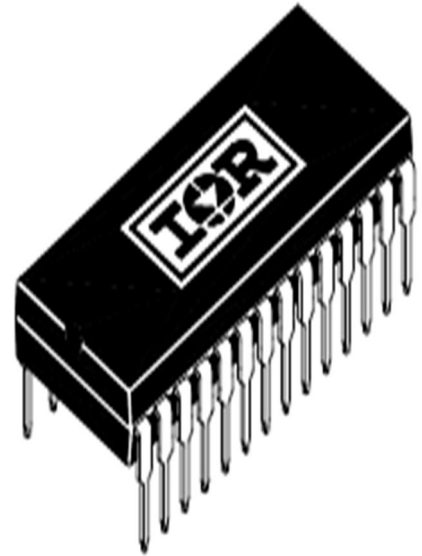
Product Summary

- Voffset   600V or 1200V max
- IO +/-   200 mA /420mA
- Vout   10 – 20 V
- Ton/toff   750/720 ns
- Deadtime   200ns.
- VCC   10 - 20 V
- VSS   5V

Lead Assignments and typical connection
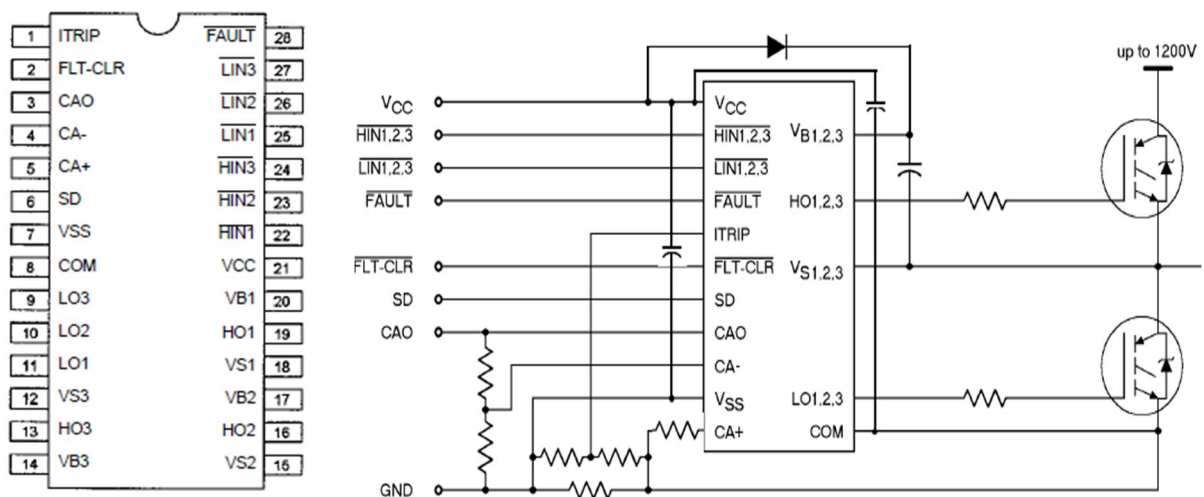
Appendix E: DC link capacitor selection

In grid connected PV system a DC link capacitor is required in order to limit the DC voltage ripples. The DC link capacitor is sized according to the following equations:

Assuming the grid voltage and the grid current are:

$$v_g(t) = V_g \cos(\omega_g t) \tag{1}$$

$$i_g(t) = I_g \cos(\omega_g t - \varphi) \tag{2}$$

Then the instantaneous output power can be easily obtained as:

$$P_{out}(t) = V_g I_g \cos(\omega_g t) \cos(\omega_g t - \varphi) = V_g^{rms} I_g^{rms} \cos\varphi + V_g^{rms} I_g^{rms} \cos(2\omega_g t - \varphi) \tag{3}$$

This can be rewritten as:

$$P_{out}(t) = S \cos\varphi + S \cos(2\omega_g t - \varphi) \tag{4}$$

Where S is the apparent power. Then assuming (i) The instantaneous input power equals to the instantaneous output power of the inverter, (ii) the DC capacitance filters out the high switching frequency components in the DC current $i_{dc}(t)$, and (iii) the DC-link has a nominal voltage of V_{dc}^n

$$V_{dc}^n * i_{dc}(t) \approx S \cos\varphi + S \cos(2w_g - \varphi) \tag{5}$$

The $i_{dc}(t)$ can be separated as a DC component, I_{dc} and an AC component, $i_{dc,ripple}(t)$.
Then the double-line frequency component can be extracted such that:

$$V_{dc}^n * i_{dc,ripple}(t) = S \cos(2\omega_g t - \varphi) \tag{6}$$

Rearranging the above equation yields:

$$i_{dc,ripple}(t) = \frac{S}{V_{dc}^n} \cos(2\omega_g t - \varphi) = I_{dc,ripple} \cos(2\omega_g t - \varphi) \tag{7}$$

Then the capacitance of the DC-link capacitor can be easily obtained given the magnitude of the maximum allowed ripple voltage, $V_{dc,ripple}^{max}$:

$$C_{dc} = \frac{I_{dc,ripple}}{2w_g * V_{dc,ripple}^{max}} = \frac{S}{2w_g * V_{dc}^n * V_{dc,ripple}^{max}} \tag{8}$$

Appendix D: PV panel characteristics (SUNTECH STP050D-12MEA)

The product dimensions and IV PV characteristics are shown in figure D.1.
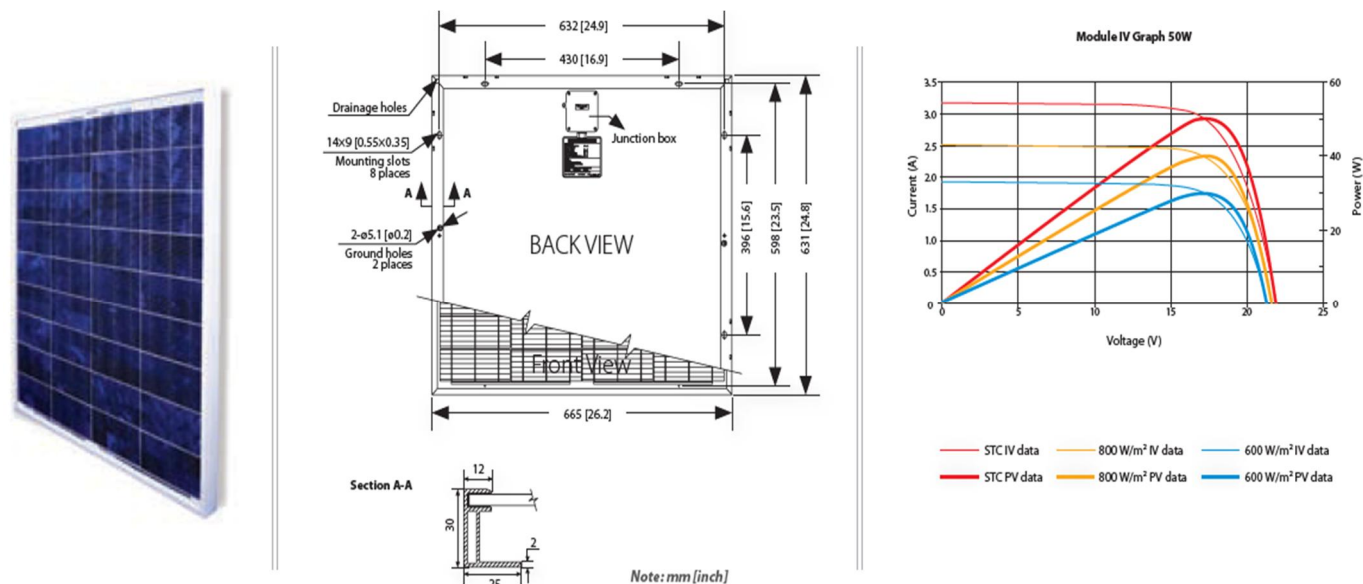
Figure D.1 (SUNTECH STP050D-12MEA) product dimensions, I-V and P-V characteristics.

The module electrical and mechanical characteristics are shown in **figure D.2.**

ELECTRICAL CHARACTERISTICS			MECHANICAL CHARACTERISTICS		
Open-Circuit Voltage (Voc)	21.6 V		Solar Cell	Mono-crystalline solar cell	
Optimum Operating Voltage (Vmp)	17.4 V		No. of Cells	36 (4×9)	
Short-Circuit Current (Isc)	0.32 A		Dimensions	216 × 306 × 18 mm	
Optimum Operating Current (Imp)	0.29 A		Weight	0.8 kgs	
Maximum Power at STC (Pmax)	5 Wp		Junction Box	IP65 rated	
Operating Temperature	-40°C to +85°C		Output Cables	(Optional cable available)	
Maximum System Voltage	715 V DC		Nominal Operating Cell Temperature (NOCT)	45±2°C	
Maximum Series Fuse Rating	5 A		Temp. coefficient of Pmax	-0.48 %/°C	
Power Tolerance	±10 %		Temp. coefficient of Voc	-0.34 %/°C	
			Temp. coefficient of Isc	0.037 %/°C	

Figure D.2 (SUNTECH STP050D-12MEA) characteristics

1- Introduction

Renewable energy, and in particular power generation from solar energy using Photovoltaic (PV) has emerged in the last decades.

The term photovoltaic ("photo" :light , "voltaic" :electricity) means the direct conversion of photons of the incident light into direct current (DC) electrical energy using semiconductor materials such as silicon; called a solar cell.

Photovoltaic power systems are generally classified according to their functional and operational requirements, their component configurations, and how the equipment is connected to other power sources and electrical loads. The principal classifications are grid-connected systems, stand-alone systems and hybrid systems. All those concepts are discussed in this chapter.

2- Definitions (cells, modules and arrays)

An individual PV **cell** (solar cell) is a unit made of various semiconductors which delivers a certain amount of electrical power depending on the intensity of the light, and is usually quite small. To boost the output power of the PV **cells,** they have to be connected together series and/or parallel in larger units called **modules**. As one or more PV **modules** are assembled as a pre-wired, photovoltaic panels result. The **modules**, in turn, can be connected to form larger units called **arrays**; i.e. the complete power-generating unit which can be interconnected to produce more power. **Figure 2.1**.

By connecting **cells** or **modules** in series, the output voltage can be increased, while the current through all **cells** is defined by its weakest **cell**, this current results in a reduction of the maximum available power. On the other hand, the output current can reach higher values by connecting the **cells** or the **modules** in parallel. [9]
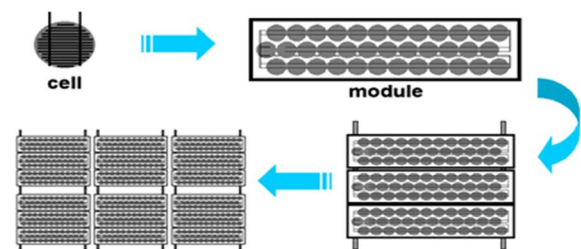
Figure2.1. Photovoltaic cells, modules, panels and arrays.

3- PV cells

The solar cell is the elementary block for the PV panels, most are made from silicon even though there are other materials such as GaAs (Gallium Arsenide), CdTe (Cadmium Telluride) and CIS (Copper Indium Diselenide CuInSe2), which vary from each other in terms of light absorption and energy conversion efficiency, as well as the manufacturing technology. All PV cells consist of two or more thin layers of semi-conducting material (p–n junction), as shown in **figure 2.2**.
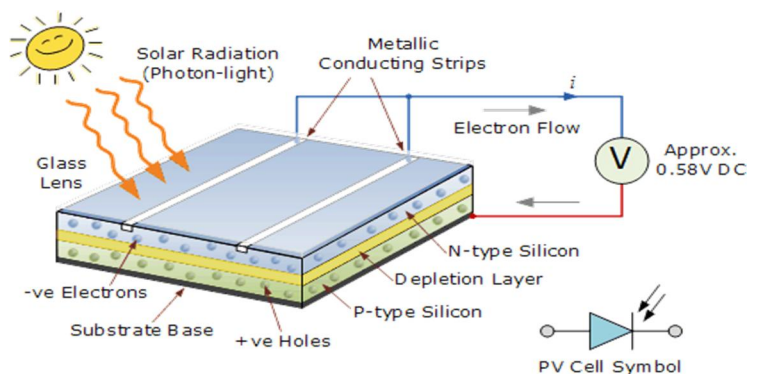
Figure 2.2 A photovoltaic cell.

When the semiconductor is exposed to light, electrical charges are generated and this can be conducted away by metal contacts as DC. The electrical output from a single cell is small, so multiple cells are connected together to form a 'string', which produces a direct current. [10]

3.1-   Cell types

PV cells can be classified pyramidally into crystalline and thin film types. Among the silicon cells, three internal crystal classes exist: Mono or single crystalline, amorphous structures and the polycrystalline structure [10, 11, 12, 13, 14, 15]. As can be shown in **figure 2.3.**
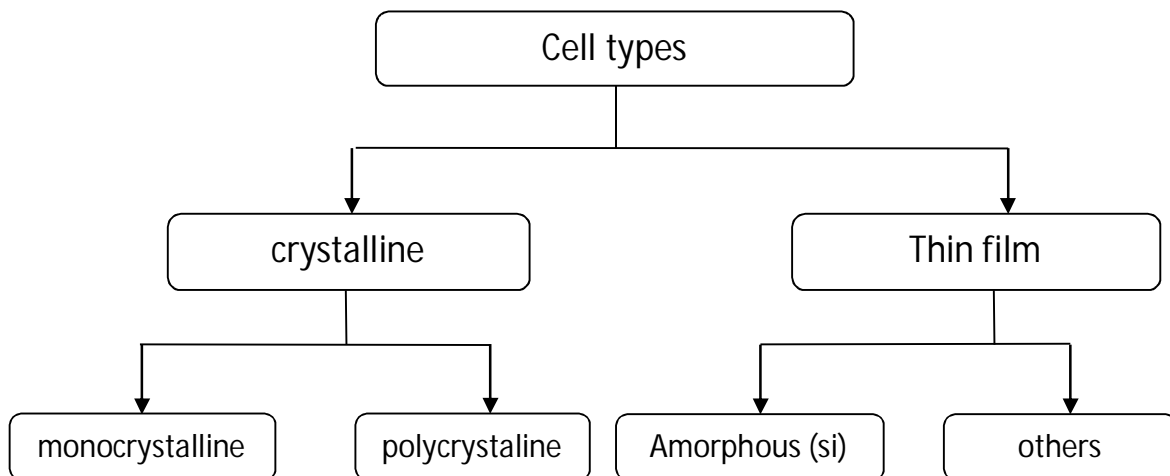
Figure 2.3 Cell types

Remark:
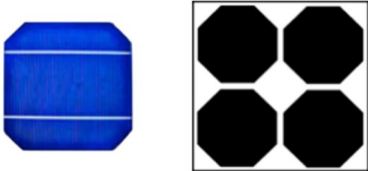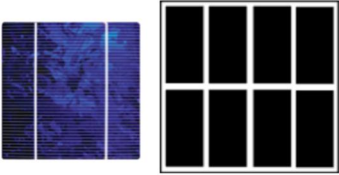
Hybrid photovoltaic cells (as shown in **figure 2.4**) are classified as PV cells that use two different types of PV technology. The Hybrid PV cell shown here is made by Sanyo and comprises a monocrystalline PV cell covered by an ultra-thin amorphous silicon PV layer. The advantage of these types of cells are that they perform well at high temperatures and maintain higher efficiencies (+18%) than conventional silicon PV cells. However, these cells come at a cost premium.
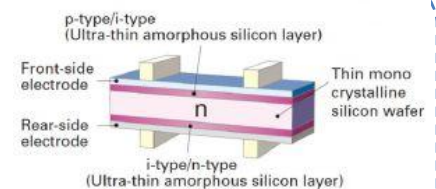
Figure 2.4 Hybrid PV cell

A brief comparison between the cell types is presented in **table 2.1**

Table 2.1 comparing the cell types

Monocrystalline Silicon (Single Silicon)	Polycrystalline Silicon (Multi-silicon)	Amorphous silicon
-Made out of what are called "silicon ingots", a very **pure type of silicon**, and a cylindrically shaped design that helps optimize performance. -Panels comprised of monocrystalline cells have rounded edges, they are **octagonal**, rather than being square. - **Most efficient** (when sunlight hits these panels at the correct angle, more of it turns into electricity) since the entire cell is **aligned in one direction** it converts around 20% of the sun's energy into electricity. - The **most space-efficient** .i.e. Solar arrays made up of monocrystalline take up the least amount of space relative to their generation intensity. - They **last the longest** of all types. -They are **more expensive** than others	-Known as **polysilicon** and **multisilicon cells**. -The silicon is melted and poured into a square mold (a **lower purity**), hence the **square shape** of polycrystalline. - They are **slightly less efficient** (13-16%). -They have a **lower heat tolerance** than monocrystalline, which means they do not perform as efficiently in high temperatures. -**Less space-efficient** -**Less expensive** to produce.	- Made by depositing silicon in a thin homogenous layer onto a substrate rather than creating a rigid crystal structure. -As amorphous silicon absorbs light more effectively than crystalline silicon, the cells can be **thinner**. Hence its alternative name of **'thin film' PV**. -Amorphous silicon can be deposited on a wide range of substrates, both **rigid and flexible,** which makes it ideal for curved surfaces or bonding directly onto roofing materials. -**Less efficient** than crystalline silicon, with typical efficiencies of around 6%, - **Easier** and **cheaper** to produce.

3.2-   Working principle

In order to go through the working principle of solar PV cells and understand it, the silicon cell was token as an example.

A typical silicon PV cell is composed of a thin wafer consisting of an ultra-thin layer of phosphorus-doped (N-type) silicon on top of a thicker layer of boron-doped (P-type) silicon. As shown in **figure 2.5**.
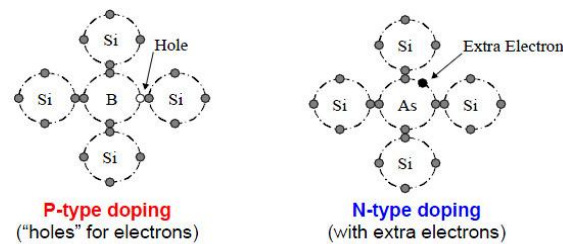
Figure 2.5 Doping of silicon

An electrical field is created near the top surface of the cell where these two materials are in contact, called the P-N junction. When sunlight strikes the surface of a PV cell, this electrical field provides momentum and direction to light-stimulated electrons, resulting in a flow of current when the solar cell is connected to an electrical load. Diagrams of PV cell are presented in **figure2.6**.
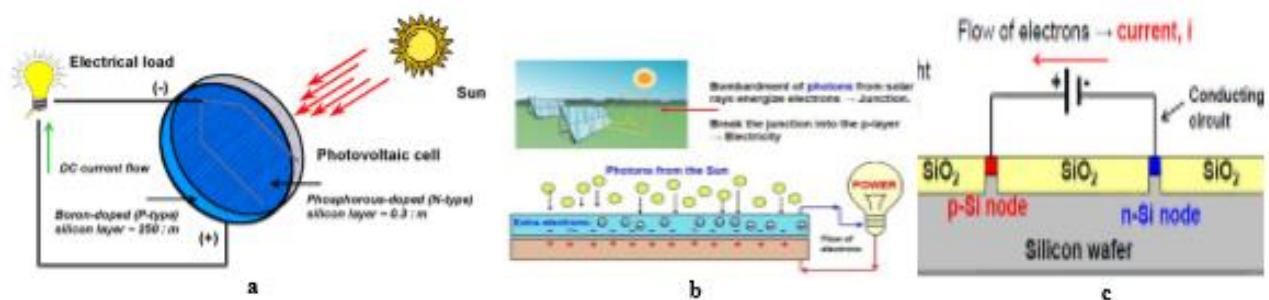
Figure 2.6 Diagrams of photovoltaic cell. a. General PV cell diagram. b.   Flow of electrons. C. flow of current from n to p junction

Regardless of size, a typical silicon PV cell produces about 0.5 – 0.6 volt DC under open-circuit, no-load conditions. The current (and power) output of a PV cell depends on its efficiency and size (surface area), and is proportional to the intensity of sunlight striking the surface of the cell. For example, under peak sunlight conditions, a typical commercial PV cell with a surface area of 160 cm^2 will produce about 2 watts peak power. If the sunlight intensity were 40 percent of peak, this cell would produce about 0.8 watt. [16]

4-   Types of PV systems

Photovoltaic power systems are generally classified according to their functional and operational requirements, their component configurations, and how the equipment is connected to other

power sources and electrical loads. The principal classifications are grid-connected systems, stand-alone systems and hybrid systems [17, 18].

4.1-   Grid connected PV systems

A grid connected or utility-interactive photovoltaic system will be interacted with utility grid. The main advantage of this system is its contribution in the energy generation and as a result the power demand satisfaction, also it makes the power system more sustainable. Grid connected systems can be designed with battery or without battery storage.

The primary component in grid-connected PV systems is the inverter, or power conditioning unit (PCU). The PCU converts the DC power produced by the PV array into AC power consistent with the voltage and power quality requirements of the utility grid, and automatically stops supplying power to the grid when the utility grid goes offline. A bi-directional interface is made between the PV system AC output circuits and the electric utility network, typically at an on-site distribution panel or service entrance. This allows the AC power produced by the PV system to either supply on-site electrical loads, or to back-feed the grid when the PV system output is greater than the on-site load demand. At night and during other periods when the electrical loads are greater than the PV system output, the balance of power required by the loads is received from the electric utility. This safety feature is required in all grid-connected PV systems, and ensures that the PV system will not continue to operate and feed back into the utility grid when the grid is down for service or repair. **Figure 2.7** presents a diagram of grid-connected PV system.
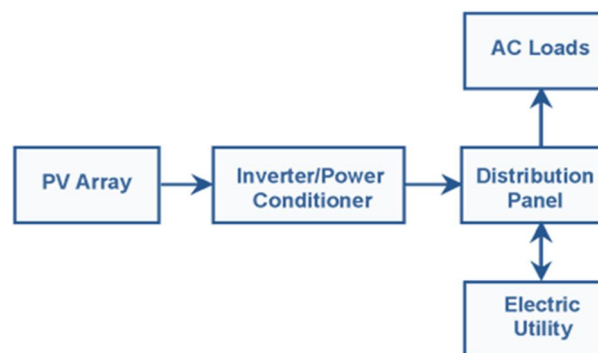
Figure 2.7 Diagram of grid-connected PV system

4.2-   Stand-alone PV systems

Stand-alone systems are designed to operate independent of the electric utility grid, and are generally designed and sized to supply certain DC and/or AC electrical loads.

The simplest type of stand-alone PV system is a direct-coupled system, where the DC output of a PV module or array is directly connected to a DC load. Since there is no electrical energy storage (batteries) in direct-coupled systems, the load only operates during sunlight hours, making these designs suitable for common applications such as ventilation fans, water pumps…etc. Matching the impedance of the electrical load to the maximum power output of the PV array is a critical part of designing well-

performing direct-coupled system. In order to extract maximum power from the PV array, DC to DC converters are required. The direct coupled PV system is shown in **figure 2.8**.

Figure 2.8 Direct coupled PV system

In many stand-alone PV systems, batteries are used for energy storage.

4.3- Hybrid systems

A system with more than one source of power is called Hybrid system. It is often desirable to design a system with additional source of power. The most common type of hybrid system contains a gas or diesel powered engine generator. Another hybrid approach is a PV/Wind system. Adding a wind turbine to a PV system provides complementary power generation as shown in **figure 2.9**.
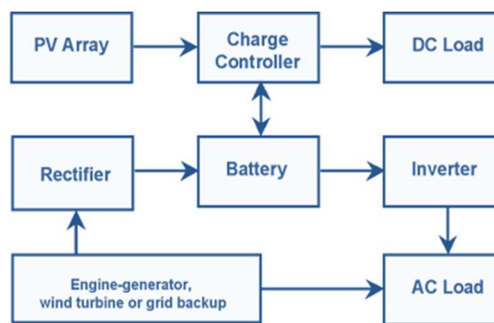
Figure 2.9 Diagram of a hybrid system

5- Conclusion

A photovoltaic system is a "new "power generating technology, it consists of using photovoltaic cells, modules or arrays interconnected to convert solar energy into electric energy.

Several types of PV cells exist, a PV cell maybe of crystalline structure or thin films. Similarly, PV Systems can be of two principal classifications; Grid Connected PV system, which is designed to operate in parallel and interconnected with the electric utility grid, or Stand-Alone PV system, that is designed to operate independently of the electric utility grid .

Photovoltaic systems have numerous and unique benefits as compared to conventional power generation technologies such as flexibility (the possibility of being used for either centralized or distributed power generation), easy expansion and even transport in some cases, their fuel (sunlight) is free, no noise or disturbance is created also they are environment friendly.

However, these kinds of systems also have inconvenients; the high cost of PV modules and equipment, and the area requirements can also be sited as a limiting factor.

Photovoltaic systems can operate normally in grid-connected mode and still operate critical loads when utility service is disrupted, this can be done under the condition of using battery storage. Under normal circumstances, the system operates in grid-connected mode, if it happens that the grid becomes de-energized, a control circuitry in the inverter will make it operate from the battery to supply power only to dedicated loads.

1-   Introduction

A PV module is the interface which converts light into electricity. Modeling this device necessarily requires taking data (irradiance and temperature) as input variables. The output can be current, voltage, power or other. However, plotting the I (V) or P (V) characteristics needs these three variables. Any change in the entries immediately implies changes in outputs. That is why, it is important to use an accurate model for the PV module.

In this chapter a detailed modeling of a PV panel is presented and simulated using MATLAB/Simulink software due to its frequent use and its effectiveness.

2-   The electric model of PV cell & array

The number of unknown parameters increases when the equivalent circuit of the chosen model becomes more convenient and far from being the ideal form. But most of the manufacturers' data sheets do not give enough information about the parameters which depend on weather conditions (irradiance and temperature). So, some assumptions with respect to the physical nature of the cell behavior are necessary to establish a mathematical model of the PV cell and the PV module, combined with the use of information given by the constructors. Some electric models are given bellow [19].

> ➢ The ideal single diode model.
> ➢ Single diode with R_s model.
> ➢ Single diode with R_s and R_p model.
> ➢ Double diode model.

2.1-   Definitions of key parameters

The photo current (I_{ph}) The current in the cell that results from solar radiation is called the photocurrent which flows in the direction opposite of the forward dark current. Its value remains the same regardless of external voltage and therefore it can be measured by the short circuit current. The photocurrent mainly depends on the solar irradiation and cell's working temperature[19], which is described as:

$$I_{Ph} = I_{sc} + K_I(T_C + T_{Cref})\frac{G}{G_{ref}} \tag{3.1}$$

Where
$$I_{sc} = I_{sc,ref}\frac{G}{G_{ref}} \tag{3.2}$$

$$K_I = \frac{I_{sc} - I_{sc,ref}}{T_c - T_{ref}} \tag{3.3}$$

Where: **G**: the actual irradiance (W/m^2).

     G$_{ref}$: the reference irradiance at STC=1000 (W/m^2).

     K$_I$: the temperature coefficient of short-circuit current (A/°K).

     T$_C$,T$_{Cref}$:the actual and reference temperature conditions (°K).

The saturation current (I_0 or I_s) known as the reverse diode saturation current and it's a function of (T)[19].

$$I_S = I_{s,ref}\left(\frac{T_C}{T_{cref}}\right)^3 \exp\left[\left(\frac{qE_g}{KA}\right)\left(\frac{1}{T_{cref}} - \frac{1}{T_C}\right)\right] \tag{3.4}$$

Where: **Eg:** material band-gap energy (1.12 eV for Silicon) and $I_{s,ref}$ (the reverse saturation current at STC implementation) is given by:

$$I_{s,ref} = \frac{I_{SC,ref}}{\exp\left(\frac{q\,V_{OCref}}{A\,K\,T_C}\right) - 1} \tag{3.5}$$

The ideality factor (A) is a constant which depends on PV cell technology and can be chosen from **Table 3.1**.

Table 3.1 Ideality factor (A)

.

Technology	Ideality factor
Si-mono	1.2
Si-poly	1.3
a-Si-H	1.8
a-Si-H tandem	3.3
a-Si-H triple	5

2.2- The ideal model

The ideal model does not take into account the internal losses of the power. A diode is connected in anti-parallel with the light generated current source. An equivalent circuit of the ideal single diode model is shown in **figure 3.1.**

Figure 3.1 Ideal single diode model equivalent circuit

The output current I_{pv} is obtained by Kirchhoff law, and is the difference between the photocurrent I_{ph} and the dark (diode) current I_D:

$$I_{pv} = I_{ph} - I_D \tag{3.6}$$

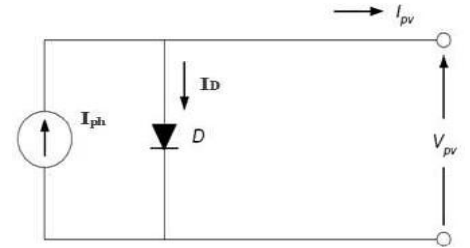The diode current I_D is proportional to the saturation current. It has an exponential characteristic given by:

$$I_D = I_S\left[\exp\left(\frac{V}{A.N_S.V_T}\right) - 1\right] \tag{3.7}$$

Where: **V** is the voltage imposed on the diode.

V_T is called the thermal voltage because of its exclusive dependence of temperature.

$$V_T = K.\frac{T_C}{q} \tag{3.8}$$

V_T = 26 mV at 300 K for silisium cell.

K   is Boltzmann constant = $1.381*10^{-23}$(J/K)

q   is electron charge =$1.602*10^{-19}$(C)

N_s: is the number of PV cells connected in series (number of cells per module).

❖   In equation (3.7), the terms N_S, A and V_T are inversely proportional to cell temperature so they vary with varying conditions. For simplicity "the modified ideality factor" is introduced:

$$a = N_S . A . VT \tag{3.9}$$

In reality, it is impossible to neglect the series resistance R_s and the parallel resistance R_P because of their impact on the efficiency of the PV cell and the PV module[19].

2.3-   The single diode with R_S model

An equivalent circuit of the single diode with series resistor model is shown in **figure 3.2**.

When the series resistance R_S is taken into consideration, equation (3.7) should take the following form:
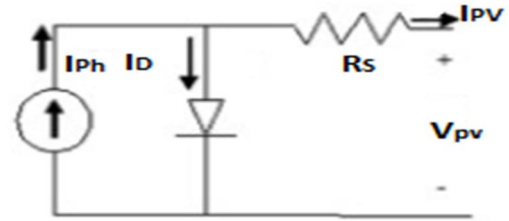
Figure 3.2 Single diode with R_s model equivalent circuit

$$I_D = I_s \left[\exp \left(\frac{V + I_{PV} R_S}{a} \right) - 1 \right] \tag{3.10}$$

❖   It is clear that previous model is simpler and easier to implement in the simulator however it is less accurate than this one. Hence, the more parameters are taken into consideration the more accurate is the representation of the PV cell[19].

2.4-   The single diode with R_S and R_p model

The single diode equivalent circuit of a PV cell with R_s and R_p is the most representative of the PV cell. It is widely used especially in simulation purposes for its simplicity and high accuracy. The circuit contains a current source which produces the photoelectric current I_{ph} and a diode in addition to a parallel resistor R_p, represents the leakage current, and a series resistor $R_{s,}$ represents the internal resistance to the current flow which produces a voltage drop. An equivalent circuit of the single diode with series and parallel resistors model is shown in **figure 3.3**.
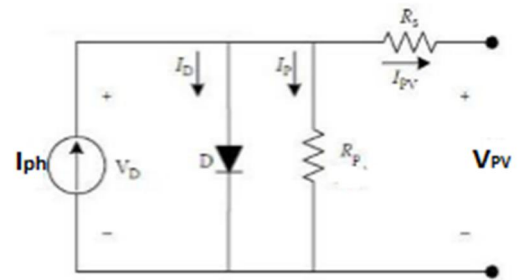
Figure 3.3 Single diode with R_s and R_p model equivalent circuit

The cell output current can be obtained simply By applying Kirchhoff's law as follows:

$$I_{PV} = I_{ph} - I_D - I_p \tag{3.11}$$

Where: I_P, is the current leak in parallel resistor.

According to the equation (3.12), the output current of a module containing N_S cells in series will be:

$$I_{PV} = I_{ph} - I_S \left[\exp\left(\frac{V + I_{PV}\, R_S}{a} \right) - 1 \right] - \frac{V + I_{PV}\, R_S}{R_p} \tag{3.12}$$

It is not easy to determine the parameters of this transcendental equation. But this model offers the best match with experimental values[19].

- ## Determination of the parameters

The number of parameters to be determined depends on the chosen model and on the assumptions adopted by the user.

In this work there are two parameters that had to be evaluated which are the photoelectric current (I_{ph}) and the reverse saturation current (I_0)[19].

a-   Determination of I_{ph}

According to the ideal model in figure 3.1 and at standard test conditions (STC) the output current is given by:

$$I_{PV} = I_{ph,ref} - I_{s,ref} \left[\exp\left(\frac{V}{a_{ref}} \right) - 1 \right] \tag{3.13}$$

This equation allows quantifying $I_{ph,ref}$ which cannot be determined otherwise. When the PV cell is short-circuited:

$$I_{sc,ref} = I_{ph,ref} - I_{s,ref} \left[\exp\left(\frac{0}{a_{,ref}} \right) - 1 \right] = I_{ph,ref} \tag{3.14}$$

However, this equation is valid only in the ideal case. So, in the reality this equality is not correct. And then, equation (3.14) must be rewritten as:

$$I_{ph,ref} \approx I_{sc,ref} \tag{3.15}$$

The photocurrent depends on both irradiance and temperature:

$$I_{ph} = \frac{G}{G_{ref}} (I_{ph,ref} + K_I \cdot \Delta T) \tag{3.16}$$

Where: $\Delta T = T_c - T_{c,ref}$ (Kelvin).

$T_{c,ref}$: cell temperature at STC = 25+273 = 298 K.

$I_{ph,ref}$: the photocurrent (A) at STC.

b- Determination of I_s

The shunt resistance R_p is generally regarded as great, so the last term of the relationship (3.13) should be eliminated for the next approximation. By applying equation (3.13) to the three most remarkable points at STC: the voltage at open circuit (I =0, V= $V_{oc,ref}$), the current at short circuit (V =0, I= $I_{sc,ref}$), and the voltage ($V_{mp,ref}$) and current ($I_{mp,ref}$) at maximum power[19], the following equations can be written:

$$I_{SC,ref} = I_{ph,ref} - I_{s,ref} \left[\exp\left(\frac{I_{sc,ref} \cdot R_S}{a_{ref}} \right) - 1 \right] \tag{3.17}$$

$$0 = I_{ph,ref} - I_{s,ref} \left[\exp\left(\frac{V_{oc}}{a_{ref}} \right) - 1 \right] \tag{3.18}$$

$$I_{pm,ref} = I_{ph,ref} - I_{s,ref} \left[\exp\left(\frac{V_{pm,ref} + I_{pm,ref} \cdot R_S}{a_{ref}} \right) - 1 \right] \tag{3.19}$$

❖ The (−1) term has to be neglected because it is (very) smaller than the exponential term. According to equation (3.16), and by substituting ($I_{ph,ref}$) in equation (3.18) :

$$0 \approx I_{SC,ref} - I_{s,ref} \exp\left(\frac{V_{oc,ref}}{a_{,ref}} \right) \tag{3.20}$$

So, $I_{s,ref}$ is obtained as follows :

$$I_{s,ref} = I_{sc,ref} \exp\left(\frac{-V_{oc,ref}}{a_{,ref}} \right) \tag{3.21}$$

The reverse saturation current is defined by:

$$I_s = D\, T_c^3 \left[\exp\left(\frac{-q\, Eg}{A.K} \right) \right. \tag{3.22}$$

Where: **D:** diode diffusion factor

In order to eliminate the diode diffusion factor, equation (3.22) is computed twice; at T_c and at $T_{c,ref}$. Then, the ratio of the two equations is written as follow:

$$I_s = I_{s,ref} \left(\frac{Tc}{T_{c,ref}} \right)^3 \exp\left[\left(\frac{q\, Eg}{A.K} \right) \left(\frac{1}{T_{c,ref}} - \frac{1}{Tc} \right) \right] \tag{3.23}$$

Substituting $I_{s,ref}$ we get the following equation :

$$I_s = I_{sc,ref} \exp\left(\frac{-V_{oc,ref}}{a_{,ref}} \right) \left(\frac{Tc}{T_{c,ref}} \right)^3 \exp\left[\left(\frac{q\, Eg}{A.K} \right) \left(\frac{1}{T_{c,ref}} - \frac{1}{Tc} \right) \right] \tag{3.24}$$

Equation (3.24) presents I_s with some parameters provided by the manufacturers as ($V_{oc,ref}$, $T_{c,ref}$), others, related to the technology of the PV cell, as (A, Eg) and some constants. But ''a'' and T_c are dependent of actual temperature. That is why I_s has to be determined at real time[19].

3- Simulation of the PV model

For this simulation, the KYOCERA KC200GT array has been chosen, its parameters are shown in **table 3.2.**

Table 3.2 KYOCERA KC200GT parameters.

I_{mp}	V_{mp}	I_{sc}	V_{oc}	R_p	R_s	P_{max}	K_I	K_v
7.61A	26.3V	8.21A	32.9V	415.405Ω	0.221Ω	200W	3.18×10^{-3}A/°C	-1.23×10^{-1}V/°C

❖ The chosen array is provided by simscape library in Simulink/MATLAB 2015. As shown in **figure 3.4**, also its detailed simulation is provided in APPENDIX A.
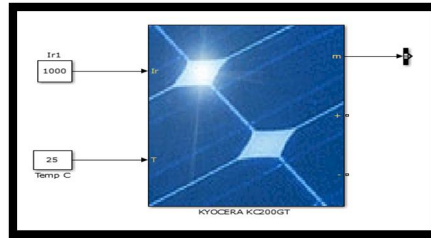
Figure 3.4 KYOCERA KC200GT array

The array has two inputs; the temperature and the irradiance. A positive and negative terminal output voltage and also an output m which is a bus that contains five parameters:

➢ The PV voltage
➢ The PV current
➢ The short circuit current
➢ The input temperature
➢ The input irradiance

Those parameters can be taken directly from the bus and used somewhere else or displayed on the scope.

The array interface, which includes all the selected array parameters, is shown in **figure 3.5**.

Figure 3.5 Simscape PV array interface

## 3.1- Output curves and discussion

Using the PV model in **figure 3.4** it is possible to plot its PV and IV characteristics simply by clicking on plot button, hence, the effect of variable irradiance and temperature on the electrical characteristics can easily be observed.

Five values of irradiance have been applied to the system from 200 W/m^2 to the SCT value which is 1000W/m^2, the $I(V)$ and $P(V)$ characteristics are shown in **figure 3.6**:
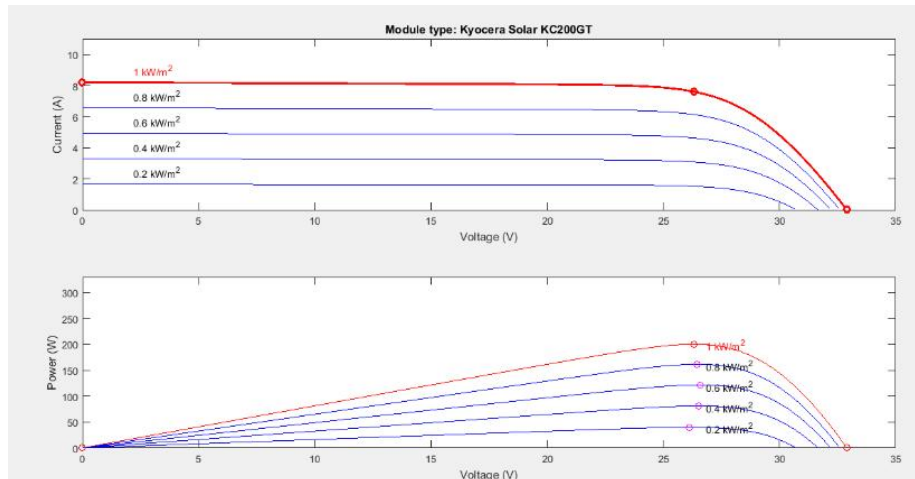
Figure 3.6 Effect of irradiance variation on the I-V and P-V characteristics.

It is clear that the irradiance affects the characteristics of the panel, this effect can be observed in those two graphs.

The output current is very sensitive to the irradiance variation, as the irradiance decreases, the current also decreases, so they are directly proportional. However, at the point where the current falls to zero the voltage doesn't change and still around the open circuit voltage.

The shape of the P(V) characteristic graph is the same for different irradiances, however, the maximum power point (shown with circles in the graph) decreases when the irradiance decreases so as in the case of the I(V) characteristic the relation is directly proportional. Also the point where the power falls to zero is around the open circuit voltage Voc.

It is very important to install the panel in appropriate location such that it is facing the sun as long time as possible, to do so, a sun tracking system may be used. In addition to that, it is necessary to measure the irradiance before installing any PV system especially in the case of PV power plants, because irradiance varies from one place to another and having some accurate statistics will help in the design of the whole system.

The second input of the PV panel is the temperature and as in the case of irradiance it is never constant, it varies by the day and during the whole year, so it is very helpful in the design to know what is exactly the effect of its variation on the output. In order to observe its effect, The PV panel in **figure 2.4** is used. The obtained results are shown in **figure 3.7**.

As it has been mentioned previously, temperature has a great effect on the output characteristics. In the case of current, increasing temperature implies decreasing the location of the critical point of the

voltage where it falls to zero and this will create a problem since it will limit the operating range of the system.

In the case of the power it is also affected by the temperature's variation, the shape of the graphs remains the same, however, it can be seen that the maximum power point is inversely proportional to the temperature, i.e. when temperature increases the maximum power decreases for example from 240 W at 0°C to approximately 120W at 80°C, also the voltage is limited up to 22V at 80°C instead of 35 V at 0°C.
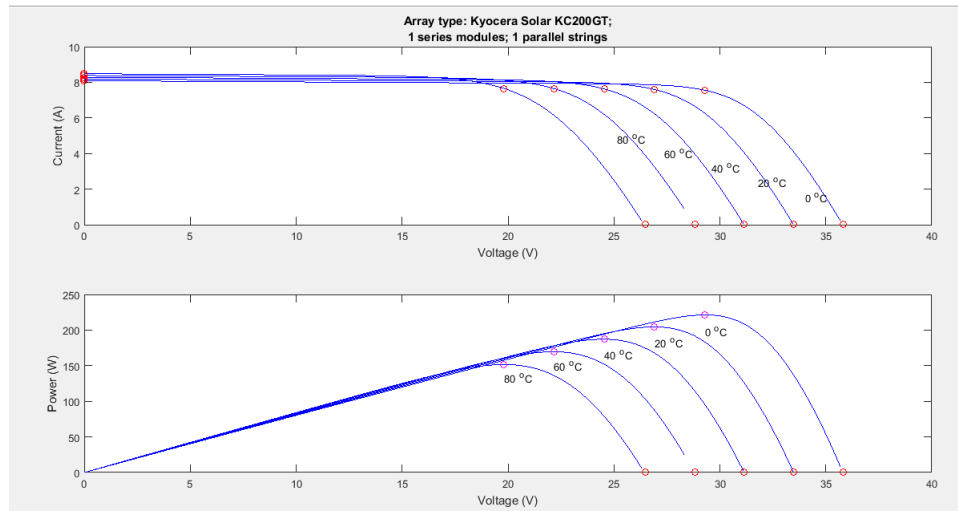
Figure 3.7 Effect of temperature variation on the I-V and P-V characteristics

3.2- Effect of Partial shading on the output characteristics

In a solar photovoltaic array and during the lifetime service, it is possible that shadow may fall over some of its cells. Under partial shading conditions the PV characteristic gets more complex with multiple peaks, hence the I-V and the P-V curves will be changed. Therefore, the system must be able to determine and absorb the maximum power from the array even in such conditions.

In order to observe the array's behavior under shading conditions, a simulation is done using four identical modules connected in series but each of which had a different irradiance value; the case of shadow. The simulation and the PV characteristics are shown in **figures 3.8** and **3.9** respectively.
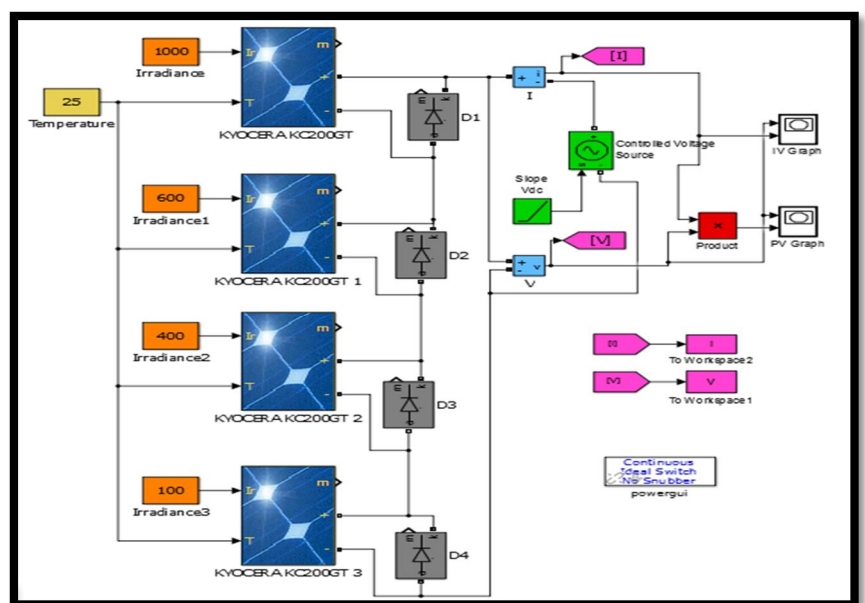
Figure 3.8 Array under shading simulation

❖ The bypass diode is used to allow current flow when the cell is damaged or shaded; it begins conducting if shading causes a cell to go far enough into reverse bias. It also allows current from non-shaded parts of the module to pass by the shaded parts and limits the effect of shading to the only neighboring group of cells protected by the same bypass diode.

The effect of shade on power output of typical PV installation is nonlinear, so that a small amount of shade on a portion of an array can cause a large reduction in output power.
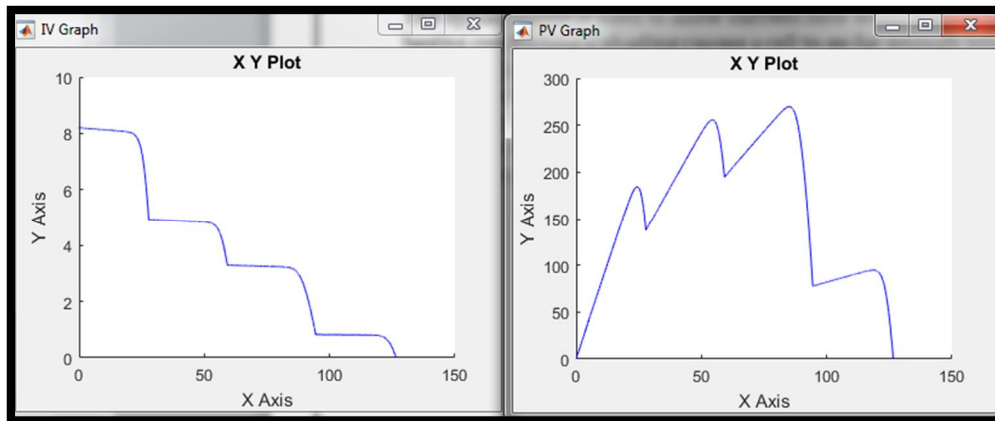
Figure 3.9 I-V and P-V characteristics

4-   Conclusion

In this chapter a detailed model of PV panel has been studied taking into consideration all the appropriate parameters.

Using the panel provided in simscape library/Simulink/MATLAB 2015 the model has been simulated and both Temperature and Irradiance variations 'effects have been shown and discussed.

Shading, one of the phenomenon that affects the array's output, has also been studied and discussed in this chapter. It has been shown that this phenomenon affects the P-V characteristic curve; it will have many peaks instead of one, hence it becomes very hard to determine where the maximum power point is located.

1-   Introduction

Grid connected Solar Photovoltaic (PV) systems are becoming very important in the PV applications field. They are composed of a photovoltaic array, DC link capacitor, single phase DC-AC inverter, filter inductor, and step up transformer for connection.

This chapter describes the design of the single phase grid connected PV system is , and complete computer simulation program of it, using Hysteresis Current Control Inverter to supply electric power to the utility grid. The simulation was developed using MATLAB/Simulink and simpower System toolbox.

2- General system description

2.1- Maximum power point tracking

The photovoltaic system has a non-linear current-voltage and power-voltage characteristics that continuously varies with irradiation and temperature (as presented in the previous chapter). In order to track the continuously varying maximum power point of the solar array the MPPT (maximum power point tracking) control technique plays an important role in the PV systems. The task of a maximum power point tracker (MPPT) in a photovoltaic (PV) system is to continuously tune the system so that it draws maximum power from the solar array regardless of weather or load conditions. Recently, various techniques have been proposed for tracking the maximum power point (MPP).

The P&O algorithm used for the studied GCPV system is the most popular MPPT algorithm, since it is much simpler and easy for implementation.

In P&O method, the MPPT algorithm is based on the calculation of the PV power and the power change by sampling both the PV current and voltage. The tracker operates by periodically incrementing or decrementing (perturbing) the solar array voltage. This algorithm is summarized in **table 4.1**.

Table 4.1 Summary of P&O algorithm

Perturbation	Change in power	Next perturbation
Positive	Positive	Positive
Positive	Negative	Negative
Negative	Positive	Negative
Negative	Negative	Positive

The algorithm works when instantaneous PV array voltage and current are used, as long as sampling occurs only once in each switching cycle. The process is repeated periodically until the MPP is reached. The system then oscillates about the MPP. The oscillation can be minimized by reducing the perturbation step size. However, a smaller perturbation size slows down the MPPT [20].

Although P&O has advantages such as simplicity and accuracy, it has some drawbacks in the case of sudden increase in irradiance; the algorithm reacts as if the increase in power is due to the perturbation, therefore the system continues the perturbation in the same direction sometimes causing the system to operate far away from the maximum power point and therefore, less efficiently.

Figure 4.1 below shows the flow chart of conventional P&O technique.
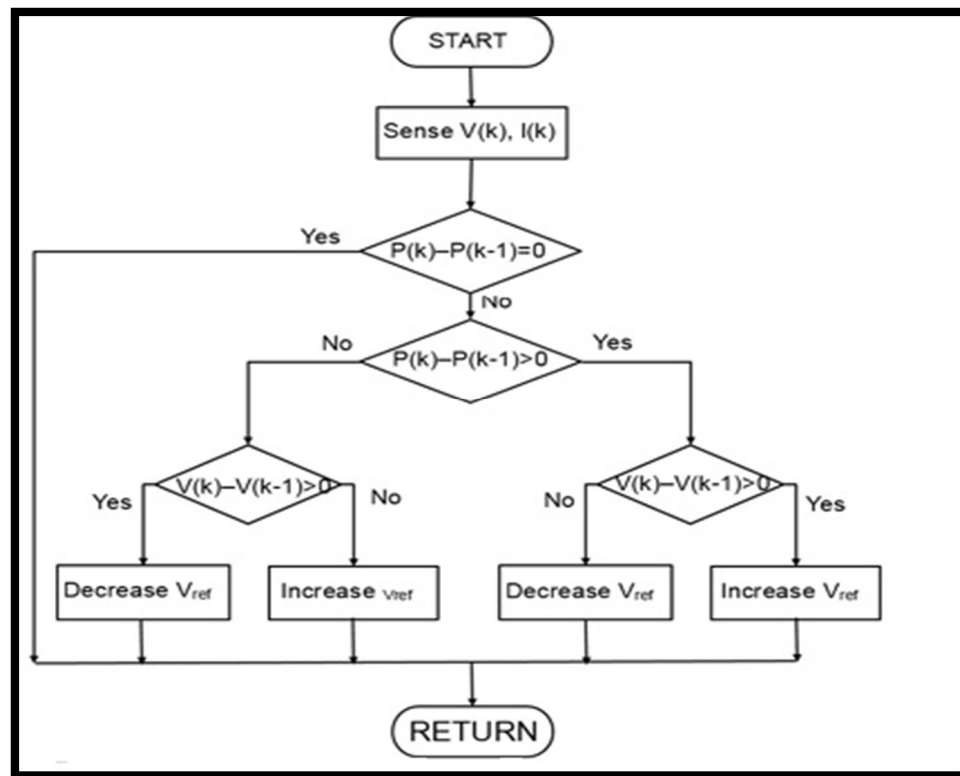

Figure 4.1 P&O flowchart[20]

Remark:

The output of the MPPT algorithm can be:

- current
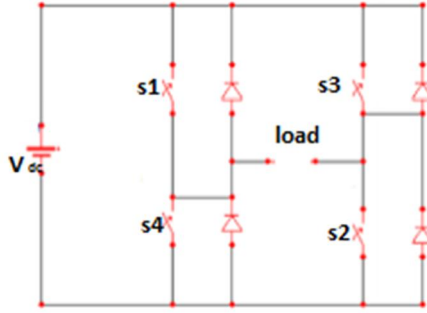- voltage
- Duty cycle

2.2-   DC to AC inverter

Inverters are electronic solid state devices used to transform electric energy from DC to AC at a desired frequency, voltage and current. Two types of inverters exist: voltage-source inverters (VSIs) and current-source inverters (CSIs):

- Voltage Source Inverter: it is the type of inverters where the independently controlled AC output is a voltage waveform. The output voltage waveform remains mostly unaffected by the load. Due to this property, the VSI have many industrial applications such as adjustable speed drives (ASD) and also in Power system for FACTs (Flexible AC Transmission).

- Current Source Inverter: it is the type of inverters where the independently controlled AC output is a current waveform. The output current waveform remains mostly unaffected by the load. This type is widely used in medium voltage industrial applications, where high quality waveform is required.

In this study, a single-phase full-bridge inverter with hysteresis current controller is modeled.

A single Phase Full wave Bridge Inverter consists of two arms, each consists of two semiconductor switches with antiparallel freewheeling diodes for discharging the reverse current. In case of resistive-inductive load, the reverse load current flows through these diodes. These diodes provide an alternative path for inductive current which continue to flow during the Turn OFF condition [21].

The simplest inverter can be accomplished with a circuit similar to the one shown in **figure 4.2**.

Figure 4.2 Single phase inverter conceptual circuit

The ideal switches in the circuit may be implemented using MOSFETS, IGBTS or bipolar transistors (depending on the power and voltage requirements). If the switches are turned ON and OFF at the required AC frequency a square wave voltage can be obtained.

The switches in each branch operate alternatively so that they are not in the same mode (ON /OFF) simultaneously .In practice they are both OFF for a short period of time called blanking time, to avoid short circuiting. They should operate in a pair as shown in **table 4.2** to get an accurate output. These bridges legs are switched such that the output voltage is shifted from one to another and hence the change in polarity occurs in voltage waveform. If the shift angle is zero, the output voltage is also zero while it is maximal when shift angle is π.

Table 4.2 Switching states of single phase full bridge inverter

Switching state	Switches ON	Switches OFF	Pulse output voltage
1	s_1, s_2	s_3, s_4	$+V_{dc}$
2	s_3, s_4	s_1, s_2	$-V_{dc}$

The circuit of the single-phase full-bridge inverter is given in **figure 4.3 (a).** The output voltage can be written as a function of the pole voltages, as

$$v_{ab} = v_{a0} - v_{b0} \tag{4.1}$$

The main waveforms of the converter are shown in **figure 4.3(b).** In this case the pole voltages v_{a0} and v_{b0} are phase-shifted by180 electrical degrees. When the pole voltages are phase-shifted of θ degrees, as shown in **figure 4.3(a)**, different modes of operation are obtained.

In Mode 1, switches S_1 and S_2 conduct the increasing positive load current ($t_0 < t < t_1$), then S_2 is turned off forcing S_1 to conduct the load current along with d_3 in a free-wheeling mode (Mode 2, $t_1 < t < t_2$) until S_1 is turned off (t_2). From this moment on, Mode 3 starts with d_3 and d_4 conducting together; the load voltage becomes negative and the load current is then forced to zero ($t_2 < t < t_3$). The zero crossing determines the beginning of Mode 4, in which the current increases in the negative direction. When S_4 is turned off, S_3 starts conducting with d_1, and so on, until the cycle is completed. [21]

Remark:

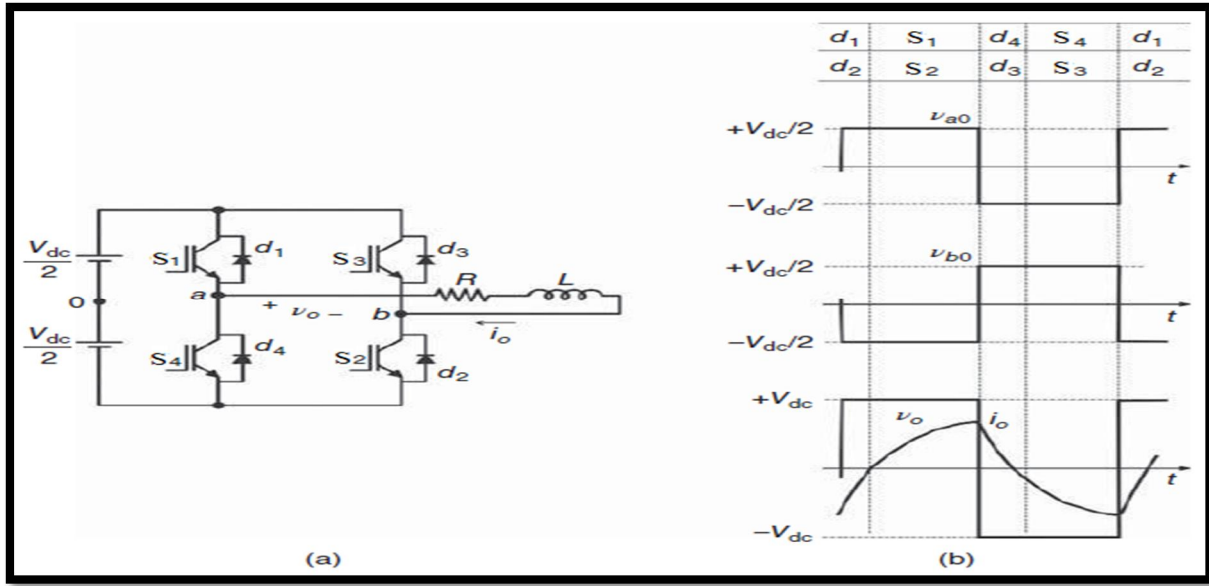   It can be observed that the AC output voltage can take values up to the DC link value v_{dc}.

Figure 4.3 (a) Single phase full-bridge inverter**. (b)** Main waveforms

       Several modulating techniques have been developed in order to drive the gates of the inverter switches among them are the PWM (bipolar and unipolar) techniques and the hysteresis band current control PWM technique as will be presented in the next section. [21]

2.3- PV Inverter control

A. Traditional control strategies

       In general, inverters are controlled by a Pulse Width Modulation (PWM) technique which is characterized by the generation of constant amplitude pulse by modulating the pulse duration, the duty cycle. The later involves turning the switches on and off multiple times per half cycle to produce a periodic symmetrical waveform.

       PWM control requires the generation of both reference and carrier signals that are fed to a comparator and it's based on some logic output, the final output is used to derive the power MOSFET switches.

       The reference signal output at the desired frequency maybe sinusoidal or square wave, while the saw tooth or triangular waves are carrier signal at a frequency significantly greater than that of the reference.

       There are various types of PWM techniques. The sinusoidal PWM (SPWM) method shown in **figure 4.4** is one of them [22].

       In order to produce a sinusoidal voltage at desired frequency say f_1, a sinusoidal control signal $V_{control}$ at the desired frequency (f_1) is compared with a triangular waveform V_{tri}. At each compare match point, a transition in PWM waveform is generated. When $V_{control}$ is greater than V_{tri} , the PWM output is high and when V control is smaller than V_{tri} , the PWM waveform is low. The frequency of the triangular waveform V_{tri} will establish the inverter's switching frequency f_s.

Figure 4.5 shows a simple circuit to produce the gating signal. No feedback or monitoring of the load current is required. The magnitude of the load current is controlled by adjusting the voltage in the DC link or the magnitude of the sine wave with respect to the triangle wave. The frequency of the load current can also be adjusted by changing the frequency of the modulating signal [22].

Figure 4.5 SPWM simple circuit implementation
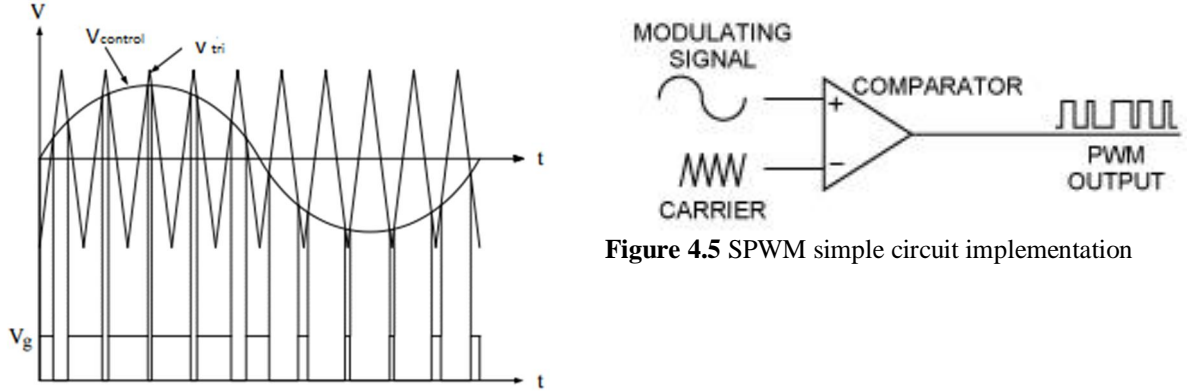
Figure 4.4 SPWM and Gating Signal

The amplitude of fundamental component of the AC voltage is:

$$V_{ac} = m * V_{dc} \tag{4.2}$$

Where m is the modulation index defined as:

$$m = \frac{V_{control}}{V_{tri}} \tag{4.3}$$

Where: $V_{control}$ is the peak amplitude of the control signal

V_{tri} is the peak amplitude of the triangle signal (carrier).

The frequency modulation ratio is also defined as:

$$mf = \frac{f_s}{f_1} \tag{4.4}$$

B. Hysteresis band current control PWM

The control method presented so far has been possible without any type of feedback. However in PV applications especially the grid connected system, feedback from the grid is required, and thus the use of a hysteresis control.

Hysteresis control (also called "bang–bang" or "tolerance band" control) uses a defined upper and lower limit based on a reference sinusoidal current waveform. The output current is monitored and maintained within certain limits of that reference waveform according to the hysteresis band.

The hysteresis band Δh defines an acceptable error in the load current based around the reference AC waveform, i_{ref}. It is defined as the difference between the upper and lower boundaries: [22]

$$\Delta h = iref + ih - (iref - ih) = 2\,ih \tag{4.5}$$

Where; i_h is a DC offset.

Figure 4.6 shows a typical non-inverting hysteresis controller waveform and its corresponding PWM output [23] .
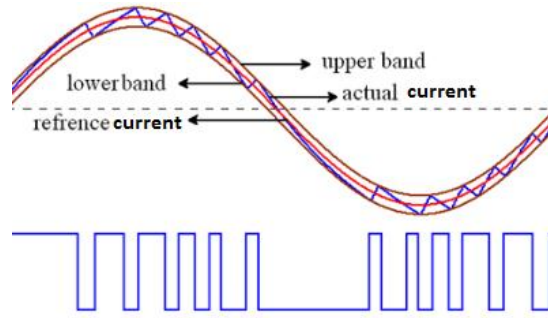
Figure 4.6 Hysteresis Controller output waveform

The inverting Hysteresis current controller contributes to the generation of the switching signals for the inverter according to the following rule.

$$
\begin{cases}
i_O < i_{ref} - \Delta h & \text{output pulse} = 1 \text{ (high)} \\
i_o > i_{ref+} \Delta h & \text{output pulse} = 0 \text{ (low)} \\
i_{ref} - \Delta h < i_o < i_{ref+} \Delta h & \text{output pulse} = \text{previous one}
\end{cases}
$$

Where i_o is the inverter's output current (the feedback current).

In the case of full bridge inverter, the magnitude of the output voltage will be V_{dc} and its frequency is obtained following the next rule:

$$
i_{ref}(t) = I_{ref} \sin(wt) \tag{4.6}
$$

In the upper band: $i_{up} = i_{ref}(t) + \Delta h$ (4.7)

In the lower band: $i_{lo} = i_{ref}(t) - \Delta h$ (4.8)

$$
\begin{cases}
\text{If } \mathbf{I_{ref} > i_{up}} & \text{the output voltage would be } -\mathbf{Vdc.} \\
\text{If } \mathbf{I_{ref} < i_{lo}} & \text{the output voltage would be } +\mathbf{Vdc.}
\end{cases}
$$

This method controls the switches in an inverter asynchronously to ramp the current through an inductor up and down so that it tracks a reference current signal.

❖ **Hysteresis band calculation**

For suitable control, the hysteresis band must be around 10% of the feedback current peak value, i.e. if the peak current is 0.7A then the upper band is at 0.035A while the lower band is at -0.035A.

2.4- Inverter to grid synchronization

Grid connected applications require an accurate estimate of the grid frequency to feed power synchronously to the grid. The phase angle of the utility is a critical piece of information for the operation

of power devices feeding power into the grid like PV inverters. There are many techniques to obtain the grid phase angle like the zero crossing detection and the orthogonal phase locked loop [24].

Orthogonal PLL is a closed loop system in which an internal oscillator is controlled to keep the time and phase of an external periodical signal using a feedback loop.

The zero crossing detection is based on converting the feedback sinusoidal grid signal to an equivalent square wave signal, compare it to the ground and generate a pulse each time a rising edge is detected; it generates an equivalent periodic pulses representing its frequency. Those pulses are used to generate an equivalent reference signal i_{ref} that will be used in the hysteresis controller.

Remark:
The measured grid voltage can be written in terms of the grid frequency (w_{grid}) as follow:

$$V = V_{grid} \sin (\theta t) = V_{grid} \sin (w_{grid}\, t + \theta_{grid}) \tag{4.9}$$

In this work a zero crossing detection technique is used. **Figure 4.7** shows the input waveform and the corresponding periodic pulses. The input voltage is in yellow, the converted square wave is in blue and the pulses are in red color.
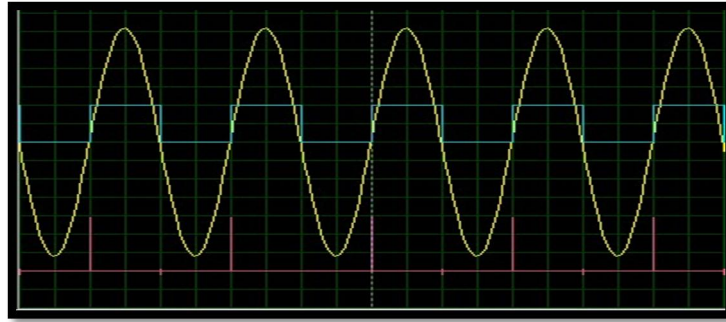
Figure 4.7 Zero crossing detector pulses

2.5- DC link capacitor selection

In grid connected PV system a DC link capacitor is required in order to limit the dc voltage ripples. The DC link capacitor is sized according to the following equation: [25]

$$C_{dc} = \frac{I_{dc,ripple}}{2w_g * V_{dc,ripple}^{max}} = \frac{S}{2w_g * V_{dc}^{n} * V_{dc,ripple}^{max}} \tag{4.10}$$

For more details refer to appendix E

Substituting, these parameters (S=200VA, f_g=50Hz, V_{dc}^{n} **= 32**V, 10% ripple which gives 3.2V) the value of the DC link capacitor can be easily calculated:

$$C_{dc} \mathbf{=} \frac{200\ VA}{2*314\frac{rad}{s}*32v*3.2v} = 3.11 \text{ mF} \tag{4.11}$$

2.6- Filter

As more PV arrays are integrated into the grid system, Power quality issues such as Total Harmonic Distortion (THD) became an increasingly serious concern since the switching devices used to convert power introduce harmonics in the system.

A. Total harmonic distortion versus total current demand distortion

The total harmonic distortion, or THD, of a signal is a measurement of the harmonic distortion present and is defined as the ratio of the sum of the powers of all harmonic components to the power of the Fundamental frequency. Hence, Current THD (Total Harmonic Distortion of the current waveform) is the ratio of the root-sum-square value of the harmonic content of the current to the root-mean-square (RMS) value of the fundamental current.

$$\text{THD(I)} = \frac{\sqrt{I_2^2 + I_3^2 + I_4^2 + I_5^2 \cdots}}{I_1} \qquad (4.12)$$

The total Current Demand Distortion TDD is the calculated harmonic current distortion against the full load (demand) level of the electrical system. At the full load TDD (I)=THD (I). So TDD gives us better insight about how big impact of harmonic distortion in our system. For example, we could have very high THD but the load of the system is low. In this case the impact on the system is also low. Therefore, Current TDD (Total Demand Distortion of the current waveform) is the ratio of the root-sum-square value of the harmonic current to the maximum demand load current.

$$\text{TDD(I)} = \frac{\sqrt{I_2^2 + I_3^2 + I_4^2 + I_5^2 \cdots}}{I_L} \qquad (4.13)$$

- According to the IEEE DR interconnection standard, IEEE-1547, any current harmonic which has an order that is greater than 35 must have a magnitude less than 0.3% of the rated current of the DR output, and the total demand distortion (TDD) has to be under 5% [26].

B. Filter types

In order to eliminate the current harmonics around the switching frequency a low-pass filter at the output is required. Ideally, filters having low cut-off frequency and high attenuation at high switching frequencies do a much better job at eliminating switching ripples efficiently. There are 3 types of filters:

1. L FILTER: The L filter is quite popular, simple to use and it has low attenuation and high inductance. The voltage drop across the inductor results in poor system dynamics, thereby leading to a long-time response. When L-filters are used, the inverter switching frequency must have a high value in order to sufficiently attenuate the harmonics [27]. Since lower attenuation of the inverter switching components is achieved by L filters, a shunt element is required in order to further attenuate the switching frequency components. A capacitor is chosen to generate low reactance at the switching frequency and to produce high magnitude impedance within the control frequency range.

2. LC FILTER: The LC-filter is best suited to such configurations where the load impedance across the capacitor is relatively high at, and above the switching frequency. The capacitance should be high to reduce cost and losses but a very high value of capacitance is not advisable, since problems such as high reactive current fed on capacitor at the fundamental frequency, inrush current, possible resonance at the grid side, and others can occur in the system. If a system is connected to the grid through an LC-filter, the resonance frequency varies over time as the inductance value of the grid varies [28].

3. LCL FILTER: In comparison with the previous filter topologies, LCL-filters can provide a better attenuation at the inverter switching frequency. They can produce a better decoupling between the filter and the grid impedance. They are able to give a good attenuation ratio even with small C and L values. However, several constraints have to be considered in designing the three-order LCL filter, such as the current ripple through inductors, the resonance phenomenon, the total filter impedance, the reactive power that the capacitor absorbs, the current harmonics attenuation at switching frequency etc [29].

C. LC filter design

In this project a second order LC filter is used. This simple configuration is easy to design and it works mostly without problems.

Figure 4.8 shows a typical LC filter configuration [30].
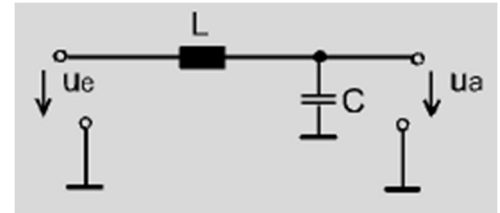
Figure 4.8 LC filter

The LC filter transfer function is:

$$\frac{Ua(s)}{Ue(s)} = \frac{1}{LCS^2+1} \tag{4.14}$$

Where the cut-off frequency is defined as:

$$\omega_c = \frac{1}{\sqrt{LC}} \quad ; \quad fc = \frac{1}{2\pi\sqrt{LC}} \quad \text{Hz} \tag{4.15}$$

And

$$Z_o = \sqrt{\frac{L}{C}} \tag{4.16}$$

Hence,

$$L = \frac{Z_0}{2\pi f_c} \text{ H} \tag{4.17}$$

And

$$C = \frac{1}{2\pi Z_0 f_c} \text{ F} \tag{4.18}$$
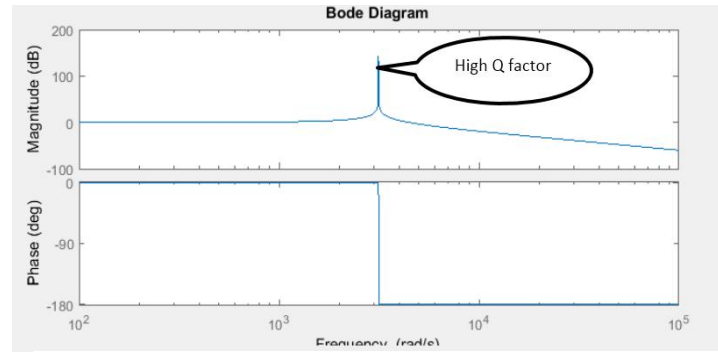
Where Zo: the LC filter characteristic impedance in ohms.
C = Capacitance in Farads.
L = Inductance in Henries.

Applying those rules to the described system yields L= 0.00318 H   and C = 0.3179 μF.

Figure 4.9 shows the bode plot of the analyzed filter.

**Figure 4.9** LC filter's Bode Plot

Discussion

The peak value appearing in the magnitude plot is due to the high Q factor. The high Q factor resulted from the assumption that no resistor is connected to the filter which is totally unreal.

The described system is marginally stable with poles on the jw axis.

When resistor values are taken into consideration, the poles move toward -∞ resulting in a stable filter.

3-   System simulation and results

MATLAB/Simulink software was used in all accomplished simulations. **Figure 4.10** shows the whole system simulated under 25C and for different irradiances from 1000 to 800W/m^2. All results are discussed below.
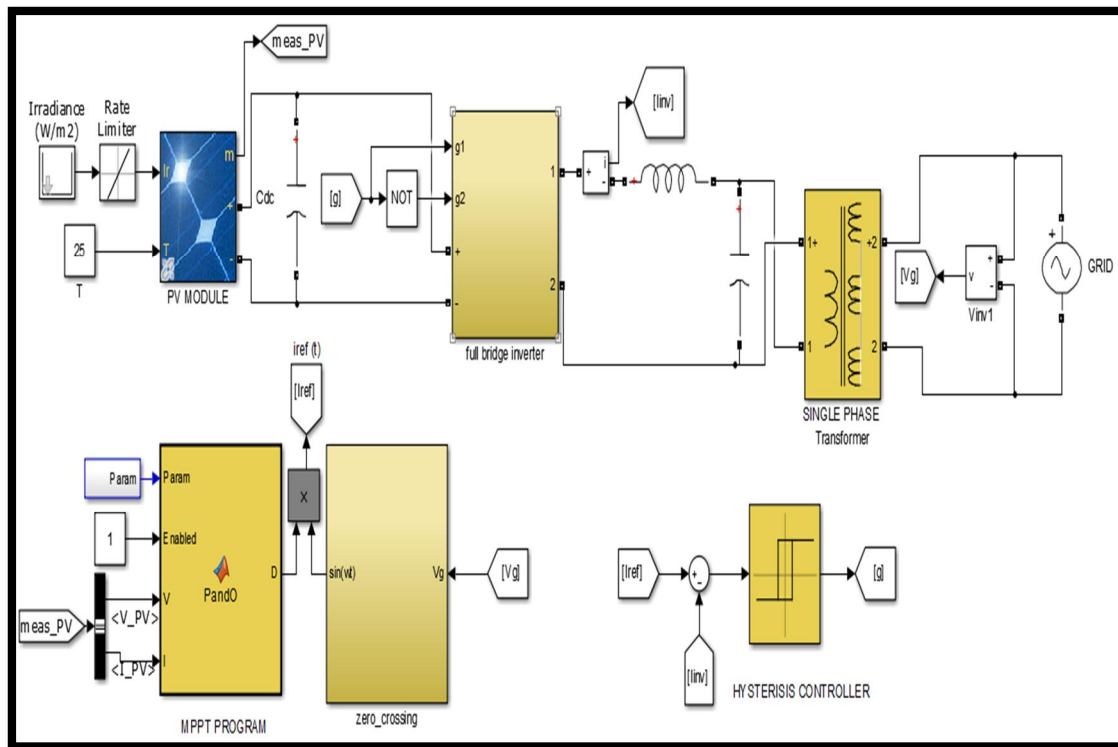


Figure 4.10 Grid connected PV system

3.1- MPP tracking

In order to test the system, different irradiances are applied (starting from 1000 W/m^2 and decreasing to 800 W/m^2).

The MATLAB program as shown in **figure 4.11** tracks the maximum power point and keep changing the duty cycle D until maximum power is obtained however it does not give an exact value but keep oscillating around it .
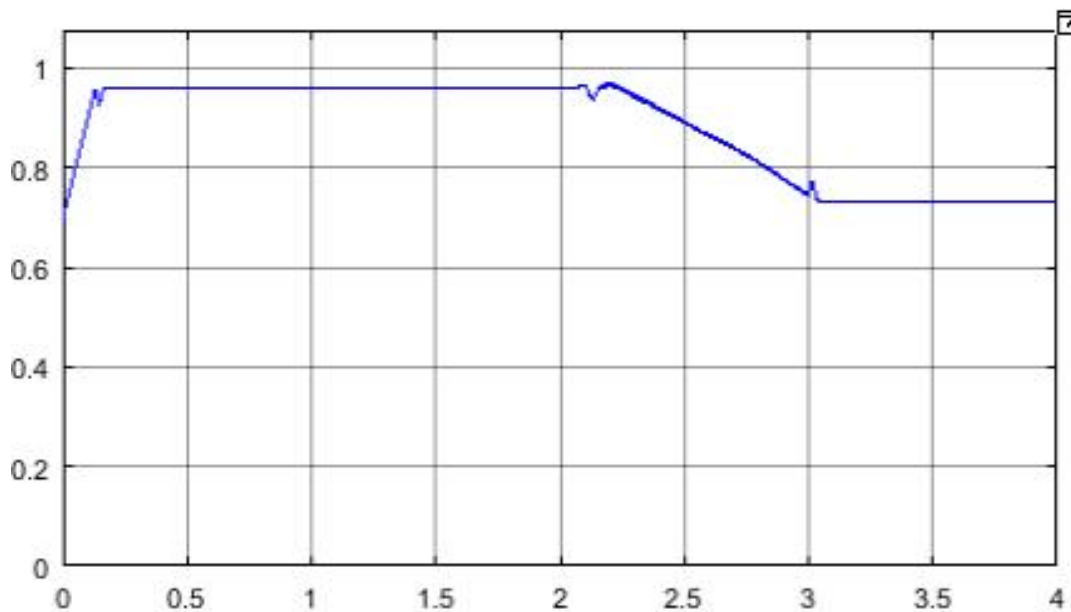

Figure 4.11 Duty cycle variation

**Figure 4.12** shows the variation of current.
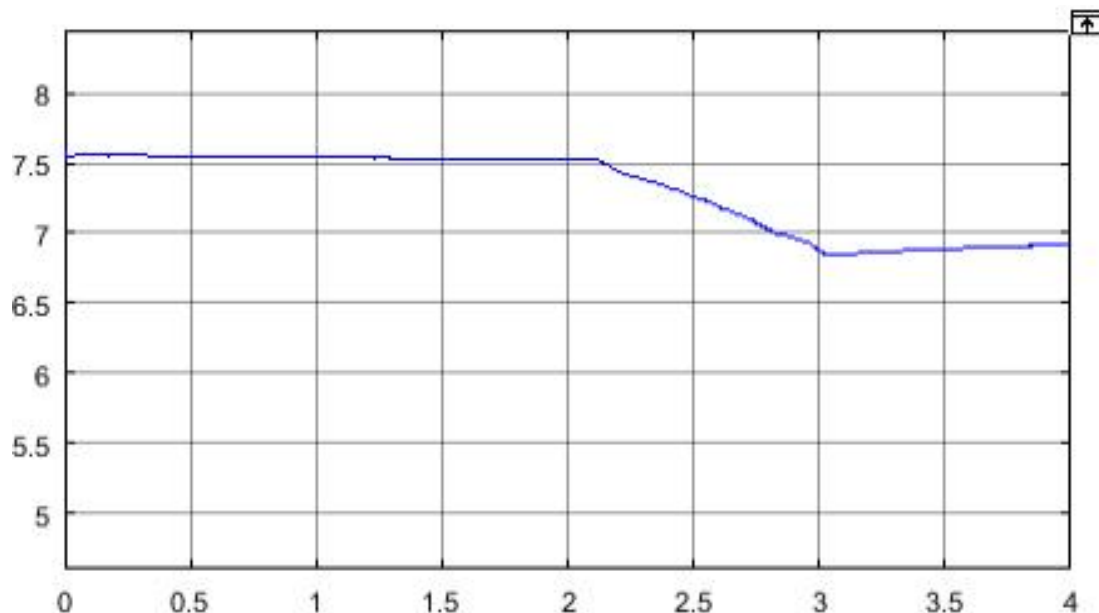
Figure 4.12 Current variation

Discussion:

- At t=0s, the irradiance was 1kW/m^2, the program calculates the suitable duty cycle which is around 0.98. The PV panel delivered a voltage of 34.2V and a current of around 7.5A resulting in maximum power during the whole period from t=0 to 2s. (**Figure 4.13**).

- When the irradiance starts decreasing at t=2s the duty cycle and the current decreases too. At t=3s, both the duty cycle and the current stabilized around 0.73 and 7.17A respectively. At that moment V= 29V resulting in a power equal to 207.93W (irradiance=800W/m^2).

- Comparing the obtained results and the theory presented in the previous section. It was concluded that the MPPT is working correctly.
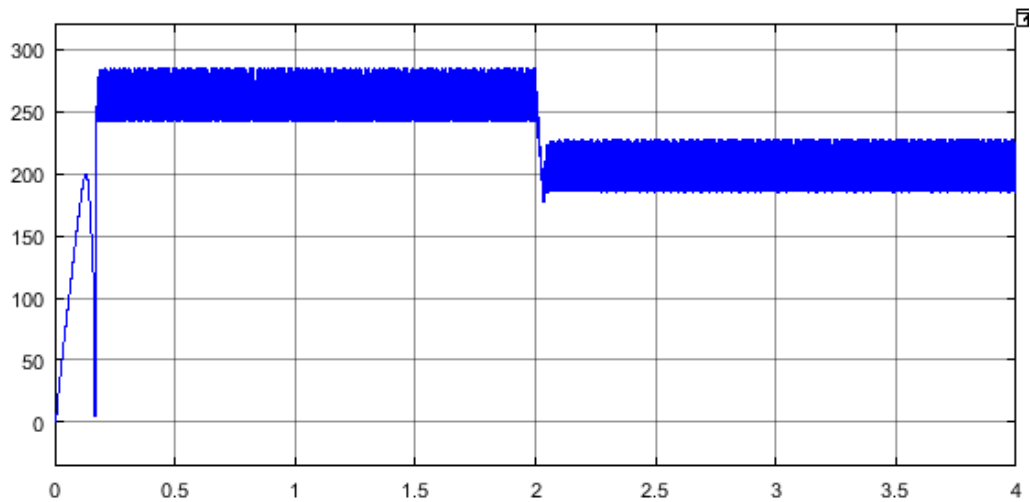

Figure 4.13 Power variation

Remark

Another validation test took place for an irradiance that changes from 1000W/m^2 to 200W/m^2 the obtained results are presented in **figure 4.14.**

(a)   (b)
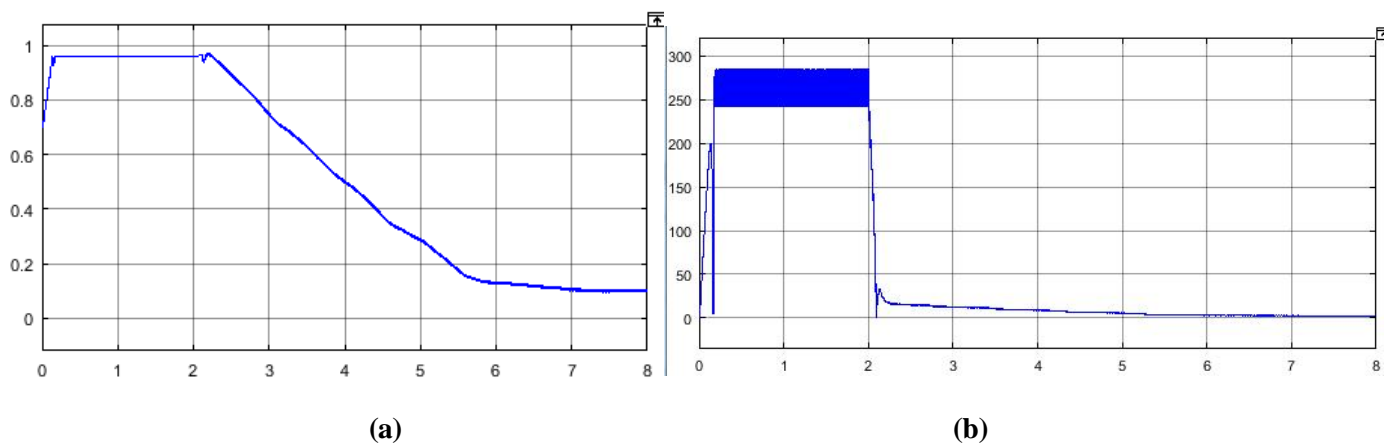
Figure 4.14 (**a**) Current and (**b**) Power variations for a change of irradiance from 1000 to 200 W/m^2

3.2-   Hysteresis controller simulation

The hysteresis controller can be implemented in Simulink using a relay block. The upper and lower limits as well as the amplitude of the output pulses can be directly set for optimum hysteresis band. The Simulink implemented hysteresis controller calculates the error between the reference and the system output currents and uses this error to generate the PWM pulses. Simulation diagram and results are shown in **figure 4.15**.

(a)   (b)
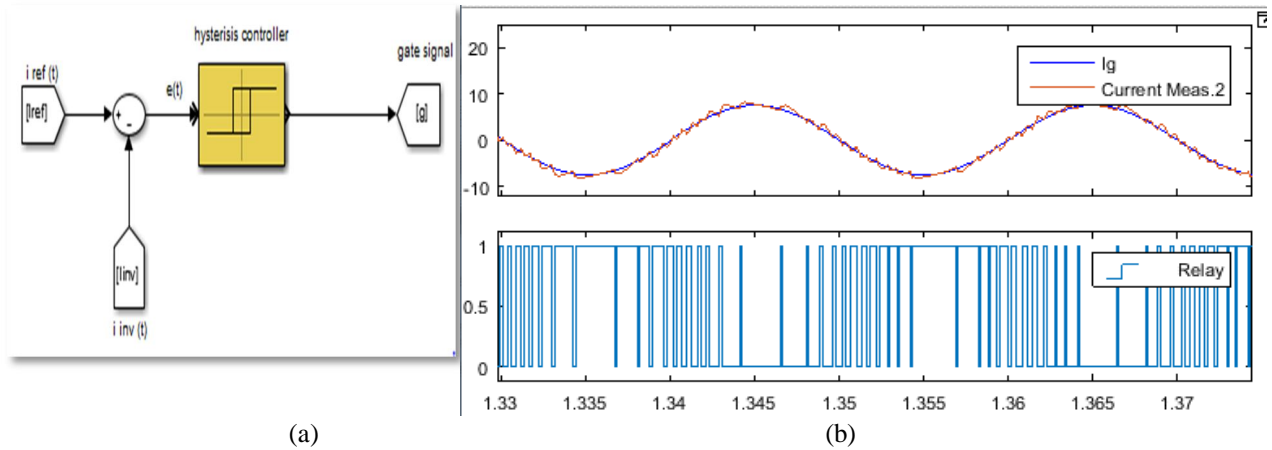
**Figure 4.15 (a)** Hysteresis Controller**. (b)** Output waveforms

3.3-   Inverter gate signal

The hysteresis controller generates a gate signal, shown in both **figures 4.15(b)** and **4.16**, with very high frequency; up to 20 KHz. This high switching frequency decreases the inverter losses and the introduced harmonics to the system as explained in the previous sections.
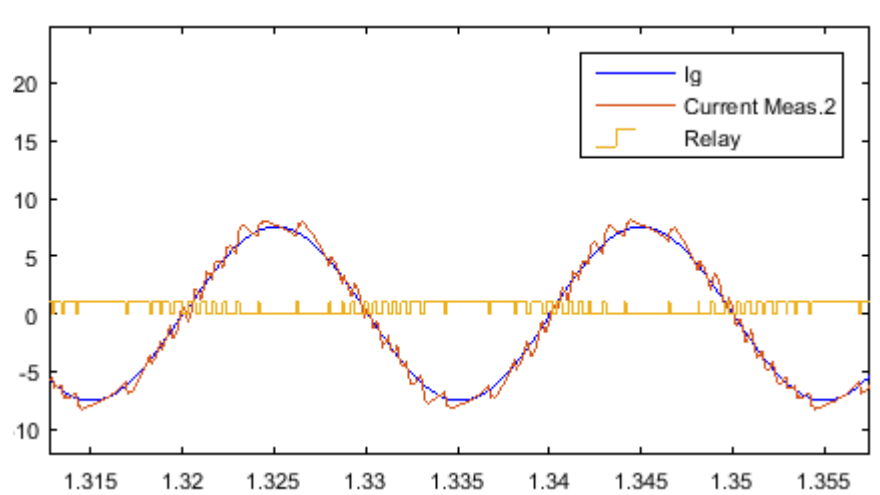
Figure 4.16 The hysteresis PWM pulses

For more details **figure 4.17** zooms the hysteresis PWM pulses.
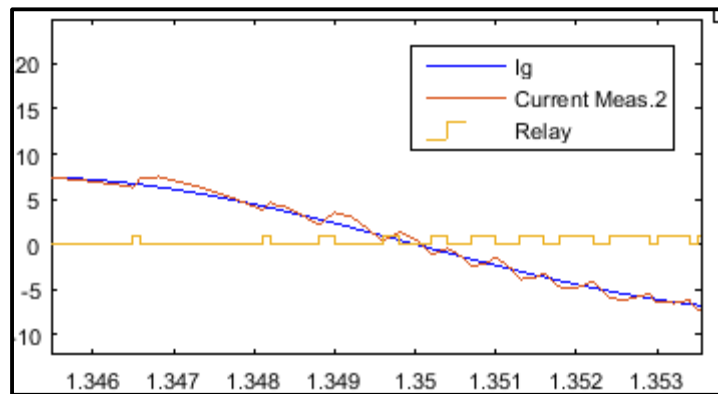

Figure 4.17 Zoom in the hysteresis PWM pulses

3.4- Zero crossing simulation

Figure 4.18 shows the Simulink model for implementing the zero crossing detector and generating the reference signal. As it was explained previously, the system receives the grid voltage and generates a reference signal having the same phase angle.

The integrator block keeps integrating the constant 314 until a rising edge is detected causing it to reset and repeat the process. The resulting waveform is periodic with the desired frequency (grid frequency) and triangular, this last is converted into a sinusoidal waveform with amplitude equals to one by passing through the sin block.
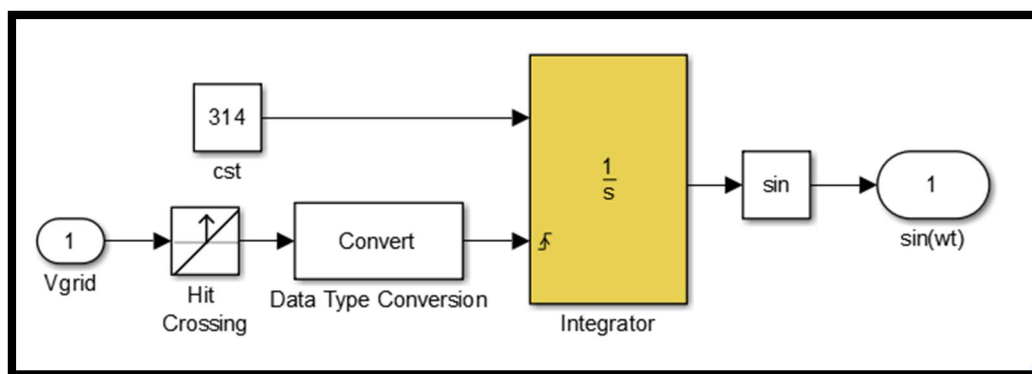
Figure 4.18 Zero crossing detector Simulink model.

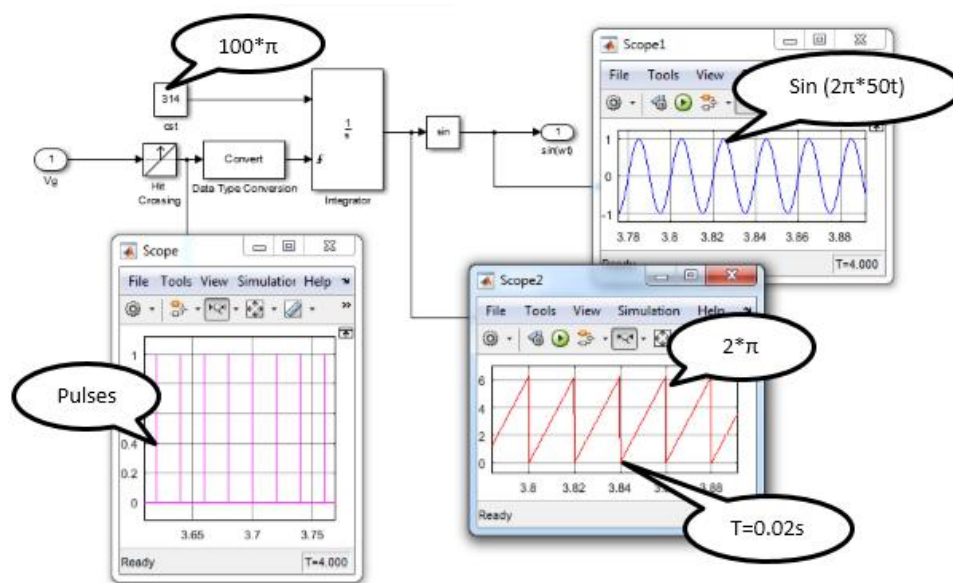**Figure 4.19** represent an explanation of the resulting waveforms.

Figure 4.19 Zero crossing detection waveforms

3.5- Inverter output analysis

In any PV system, the output voltage must be kept constant regardless of the external conditions, however, the current can vary with irradiance and temperature variation. In the presented simulation, the inverter's output voltage matches the grid's voltage in phase and magnitude but the current varies with the irradiance variation. As shown in **figure 4.20.**
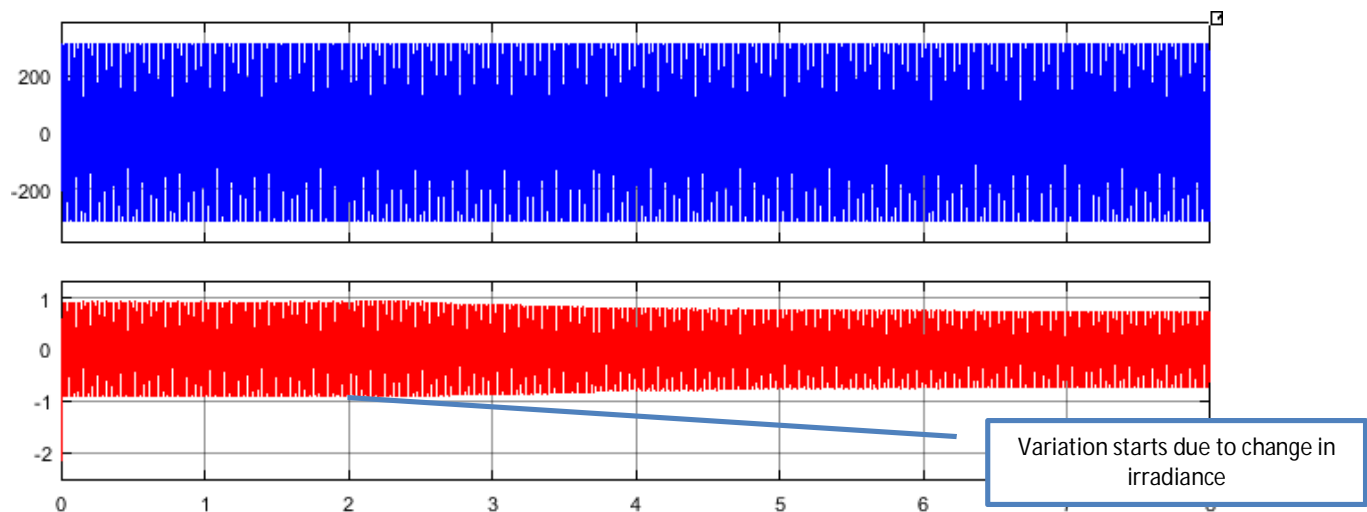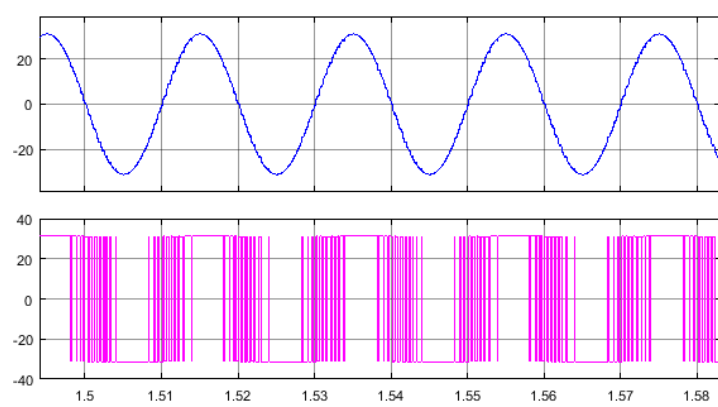

Figure 4.20 Inverter output voltage and current

When the current is in phase with the voltage, the power is positive and the inverter receives power from the grid. Since the desired functionality of this system is to generate power the current must be controlled to be out of phase by 180 degrees, resulting in negative power which means that the system supplies or injects power to the grid.

Figure 4.21 shows the inverter's voltage before and after the filtering procedure.


Figure 4.21 Inverter's voltage

Figure 4.22 (zooming **figure 4.20**) shows the output voltage to the grid versus the injected current in the case of duty cycle output from the MPPT's algorithm. While **figure 4.23** shows the output voltage to the grid versus the injected current in the case of maximum current output from the MPPT algorithm.
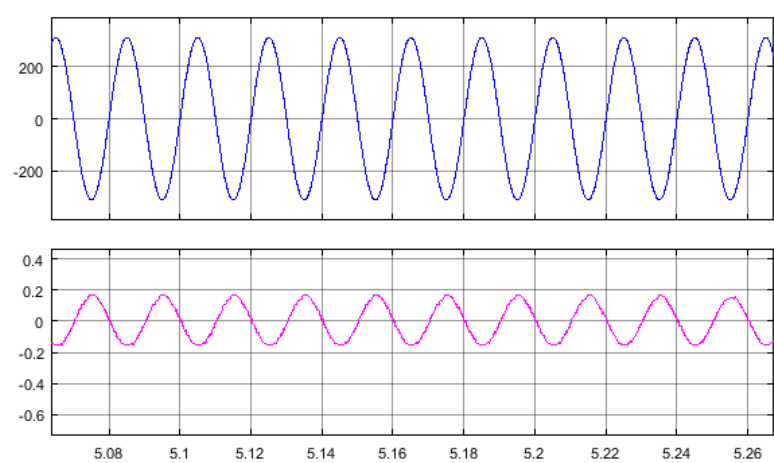
**Figure 4.22** Grid voltage versus injected current controlled by D
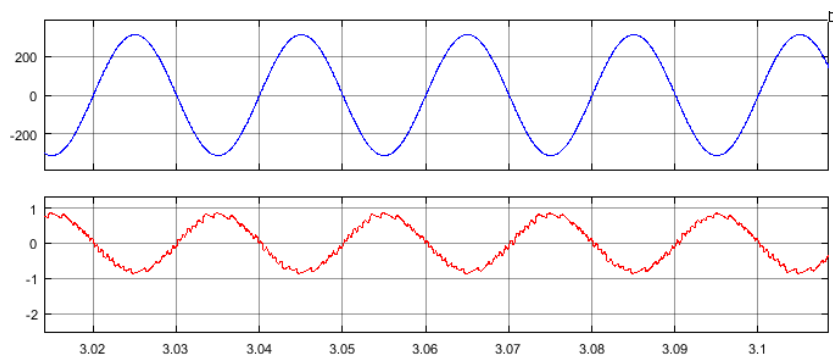
Figure 4.23 Grid voltage versus injected current controlled by I_{MPPT}

The output power quality is good; however, the amplitude is small especially in the case of duty cycle control. This small value is due to the use of only one panel, adding to it the system losses and the small reference current. In order to increase the power, either additional PV modules are added or MPPT (higher) current is used as reference, as in **figure 4.23**.

The voltage magnitude is around 311 which is the grid peak voltage and the current is 0.2A and 0.9A respectively.

3.6-   Power quality analysis

In order to observe the quality of the injected power, FFT analysis is required, the spectrum of the current and the voltage will indicate the fundamental frequency and the harmonics, **Figures 4.24 and 4.25** show the spectrum and the THD of the output voltage and current.
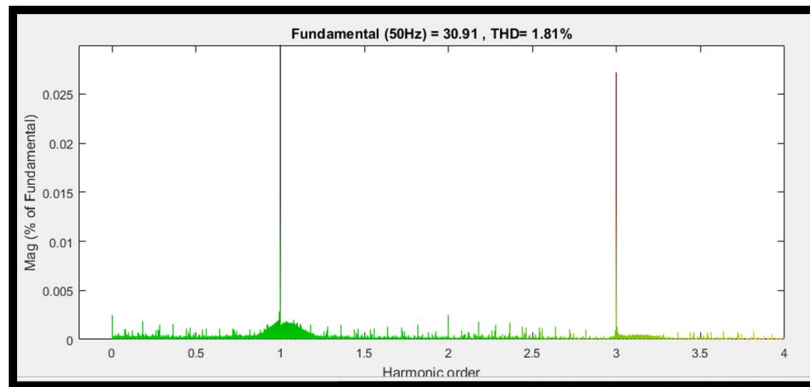
Figure 4.24 Inverter voltage spectrum
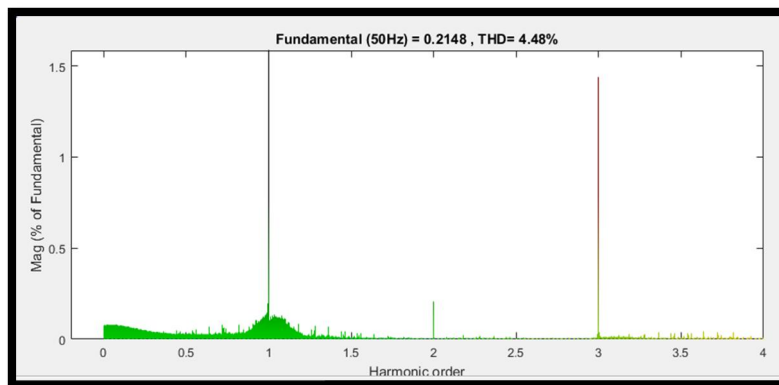
Figure 4.25 inverter current spectrum

3- Conclusion

In this chapter, a grid connected PV system has been analyzed and simulated by using MATLAB/SIMULINK. All the obtained results were discussed and explained.

The output of a solar PV power generation system is controlled via a hysteresis current controller and used to inject a power into the utility grid.   However due to the use of only one panel the inverter's output was small. Yet, for a series and parallel PV panels connection this proposed configuration can greatly satisfy the existing power demand, limit the use of conventional power generation techniques and also it is the only mean to tackle the future power requirements. It saves the fossil fuels from depletion, limits global warming and keeps the environment clean and green.

1- Introduction

The next stage after the completion of the described system's simulation is the practical implementation. That implementation must be designed according to well defined standards and specifications. The presented hardware design system, in this work, is divided into two parts: control and power circuits. Each part of the system is simulated using ISIS PROTEUS software then implemented.

In this chapter each implemented circuit is explained in details, and obtained results are discussed by the end.

2- Power supply circuit

Current sensors, op-amps, drivers and logic ICs, all need DC power supply. In general, for solar systems, DC power supplies are provided using batteries or directly from the panels. However, in this study, components are fed using the grid's power, this is due to having only one panel with low output power.

Figures below show the standard dual power supply using positive and negative voltage regulator ICs. **Figure 5.1 (a)** Represents a circuit that acts as a power supply used to generate + 15 V and – 15 V DC with a common ground. It is made of: a step down center-tape transformer, that converts the 230 V AC to 12 V AC, a Wheaston bridge, for signal rectification, 1mF smoothing capacitors C1 and C2, to remove the ripples from low volt AC, and Two regulator ICs to generate the desired voltages. This power supply is used to power amplifier circuits, current sensors in addition to the MOSFET driver IC.

Using the same method another circuit of 5 V DC is implemented, **figure 5.1 (b)**.
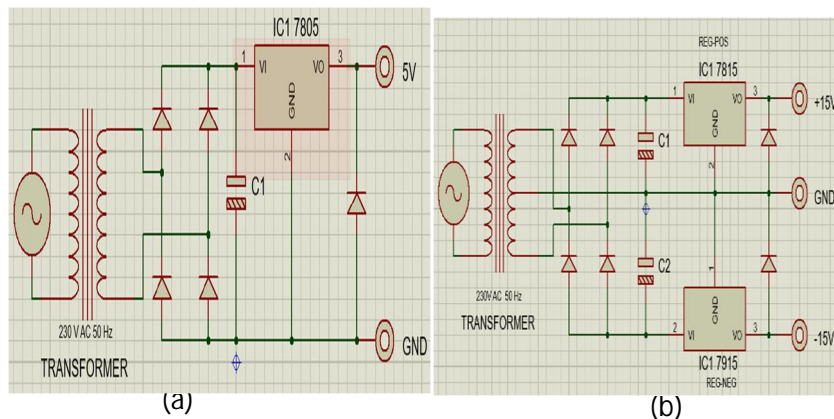
Figure 5.1 (a) 5V DC power supply. **(b)** Dual 15 V DC power supply.

The actual circuits' implementation is shown in **figure 5.2**.
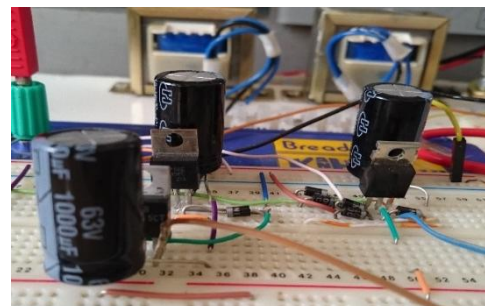
**Figure 5.2** Power supply circuits implementation.

3- Grid synchronization circuits
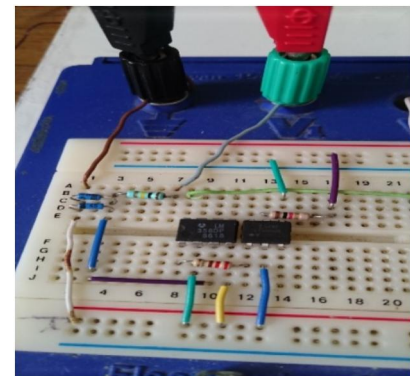
3.1- Zero crossing detector

As explained in the previous chapter, the grid synchronization is extremely important. In this implementation, a zero crossing detector circuit (which locates the rising edge of the grid's voltage and generates a periodic square wave signal in the same phase) is used for that purpose.

The periodic signal is utilized in the control algorithm, under the current sink algorithm, the Arduino microcontroller detects it as an interrupt and starts executing the rest of the program after the interrupt occurred. In other words, it is used to generate the hysteresis controller reference current.

Figure 5.3 shows the circuit topology, whereas the hardware circuit is shown in figure **5.4.**
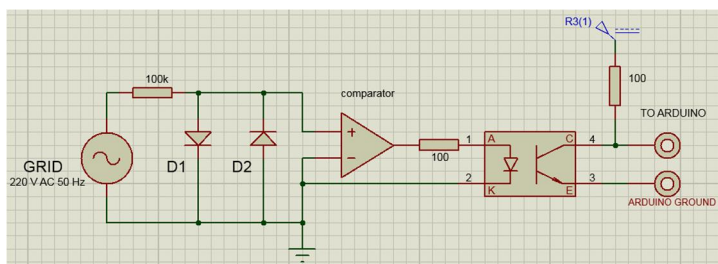
Figure 5.3 Zero crossing detector circuit

Figure 5.4 Zero crossing detector circuit actual implementation

According to **Figure 5.3**, the 100 kΩ resistor limits the current and Two Schottky diodes in parallel limit and convert the voltage to a 2-Vpk square signal.

Finally, LM358, a comparator IC, used to compare the input voltage (the positive half cycle) with the ground 0V and outputs a positive square wave signal in phase with the grid voltage.

The optocoupler L1432 is used to both send the resulting square signal to the microcontroller (Arduino due) and isolate it from the grid for protection purposes.

3.2- Sinusoidal waveform generation

In order to generate the reference current, an Arduino program is written, the program receives the square wave signal from the optocoupler and generates a sinusoidal output either in phase or out of phase with the grid's voltage.

The flowchart of the program is shown in **figure 5.5.**
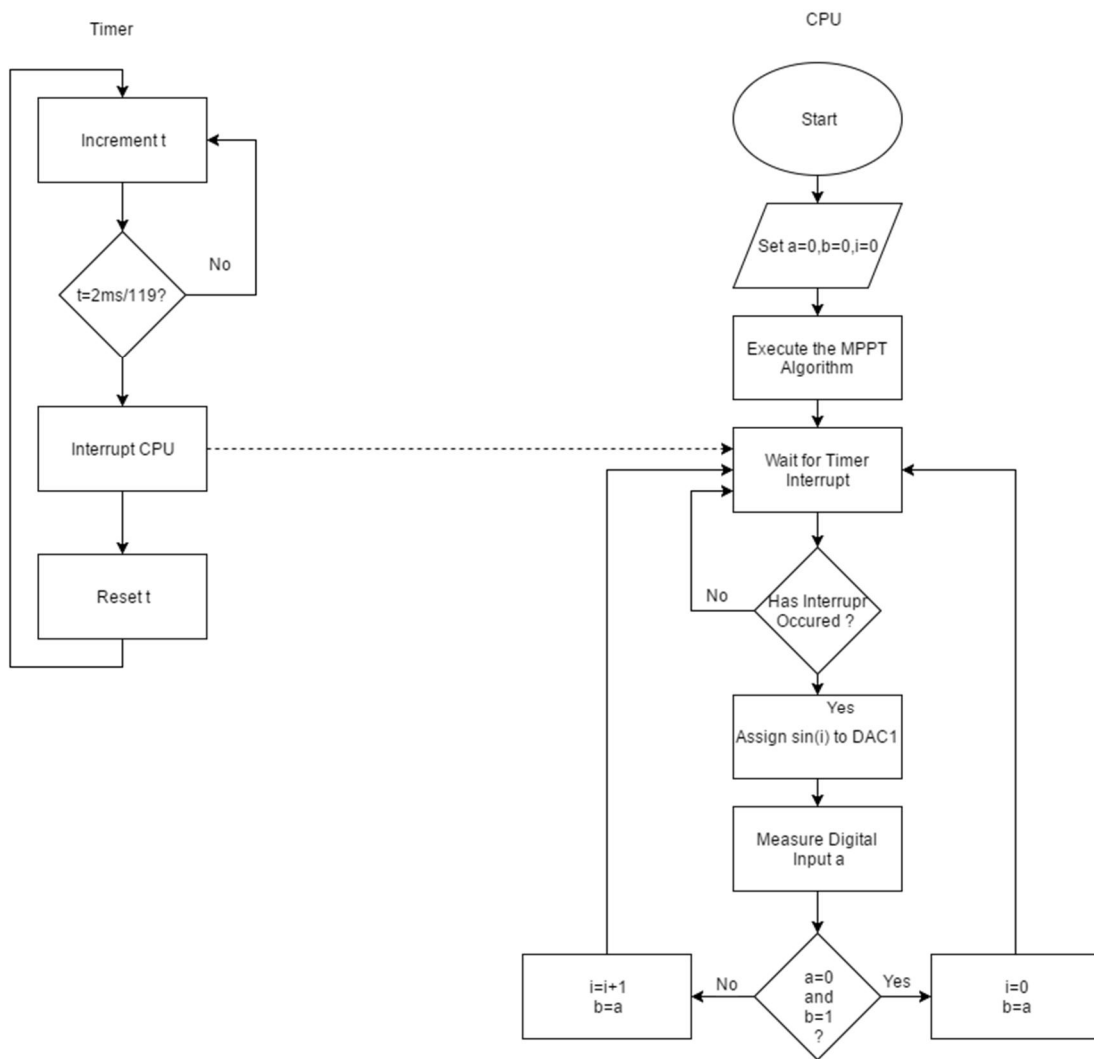
**Figure 5.5** i_{ref} generation flowchart

While the obtained reference current is in **figure 5.6** below

| **(a)** | **(b)** |
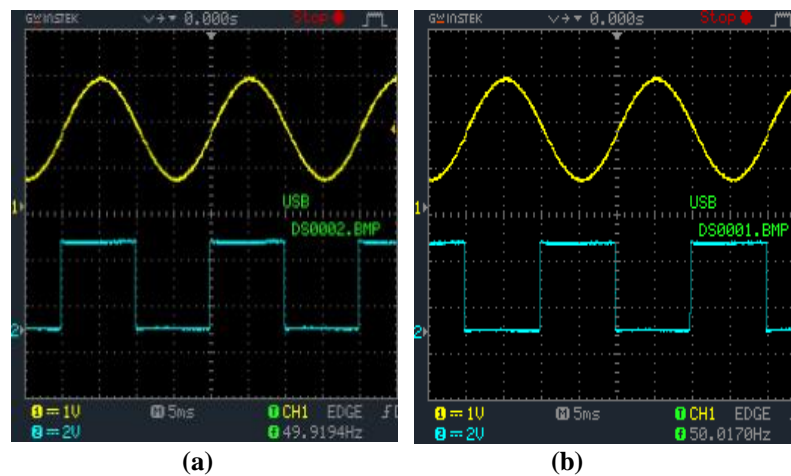
Figure 5.6 i_{ref} Arduino's output **(a)** i_{ref} in phase **(b)** i_{ref} out of phase with the grid's signal

4- MPPT implementation

The implementation of an MPPT system requires some input parameters depending on the used technique. Perturb and Observe algorithm requires, as explained in the previous chapter, the panel's current and voltage measurements in order to track the maximum power. **Figure 5.7** demonstrates the techniques used for measurements.
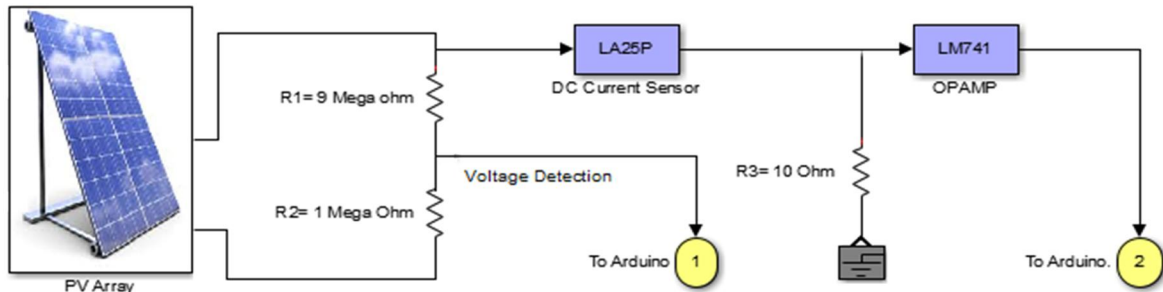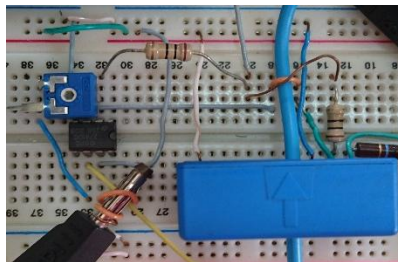

Figure 5.7 Voltage & current measurement system.

4.1- Current measurement

In order to measure the panel's output currents, a DC/AC current sensor, LA 25-P, is used. It is a closed loop Hall Effect current transducer, specifications corresponding to this component can be found in appendix B.

The sensor is supplied with the 15V dual DC power supply and generates a current of 1mA for each corresponding 1A input. This sensor has a high accuracy and a suitable range for this application. The output current is converted into voltage through a resistor of 10Ω and 100 times amplified using LM741 op-amp IC resulting in a voltage of 1V that corresponds to the 1A sensed current. This output voltage is then connected to the microcontroller (Arduino due). **Figure 5.8** shows the current sensor signal conditioning circuit.

Figure 5.8 Current sensor signal conditioning circuit

4.2- Voltage measurement

As opposed to current measurements that needs a current sensor, Voltage measurement can be done simply using a voltage divider (since the Arduino burns for an input voltage higher than 5v).

In order to reduce the losses in the system. High resistor values are used (R1= 10 MΩ and R2 = 1MΩ). The output voltage can be calculated according to the voltage divider rule shown in the following equation:

$$V_{out} = \frac{R2}{R1+R2} V_{dc} \qquad\qquad (5.1)$$

❖ Combining the MPPT's output and the generated sinusoidal signal from Arduino the reference current i_{ref} results.

5- Full bridge inverter implementation

The high switching frequency of the hysteresis current controller, that may reach 20 KHZ, requires fast switching devices. With their very high switching capability, excellent dynamic characteristics and availability of recovery diodes, four power MOSFETs, BUK 555-100A, operating in frequencies up to 2.4 MHz, are used in this work to construct the inverter.

5.1- Gate driver IC

The switching signal for a transistor is usually generated by a logic circuit, or a microcontroller, that provides an output signal, typically limited to a few milliamperes of current. Consequently, a transistor which is directly driven by such a signal would switch very slowly, with a correspondingly high power loss.

During the switching process, the transistor's gate capacitor may draw current so quickly that it causes a current overdraw in the logic circuit or microcontroller, resulting in overheating which leads to permanent damage or even complete destruction of the chip. To prevent this from happening, a gate driver is provided between the circuit's output signal and the power transistor.

Charge pumps are often used in H-Bridges (in high side drivers) for gate driving the high side n-channel power MOSFETs and IGBTs. These devices are used because of their good performance, but require a few volts above the power rail to drive its gate. When the center of a half bridge goes low the capacitor is charged through a diode, and this charge is used later to drive the gate of the high side FET gate a few volts above the source or emitter pin's voltage so as to switch it on. This strategy works well provided the bridge is regularly switched and avoids the complexity of having to run a separate power supply and permits the more efficient n-channel devices to be used for both high and low switches.[31]

In this work IOR2135 gate driver IC is used, it contains three internal drivers, it can drive up to six switching devices. However, for the full bridge topology only two of them are used.

MOSFET and driver characteristics can be referred to in appendix C whereas the hardware implementation is shown in **figure 5.9.**
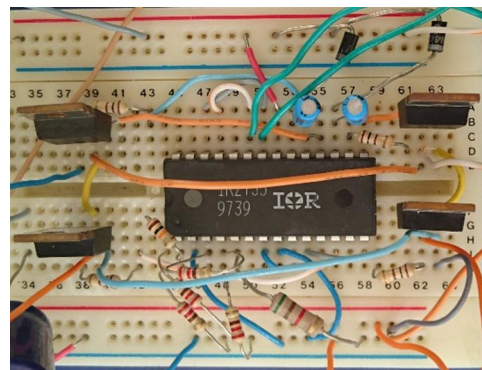
Figure 5.9 Full bridge inverter implementation

5.2-   Dead time generation

Due to the very high switching frequency, it is difficult to avoid the state where all switches are turned ON. Although its period is very small (in terms of Nano seconds), short circuits may be caused, resulting in a damage of the inverter. In order to avoid this state, a dead-time, or delay, of 0.2µs is implemented using NAND gates. The circuit topology is shown in **figure 5.10.**
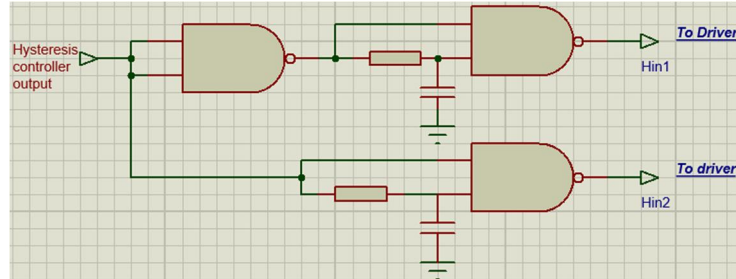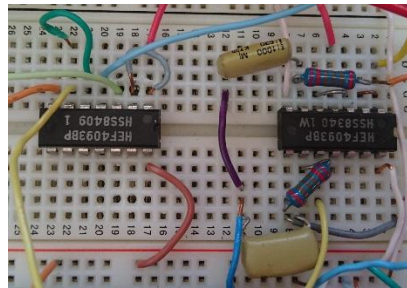

Figure 5.10 Dead-time circuit topology

With R = 2KΩ and C = 1nF, the introduced time delay is given by:

$$t_{delay} = \mathbf{R \times C} = \mathbf{2k\Omega \times 1nF} = 2\mu s \tag{5.2}$$

Using CD4093B IC, the circuit is implemented and shown in **figure 5.11**.

Figure 5.11 Dead-time circuit implementation

6- Hysteresis current control implementation

In order to generate the inverter's duty cycle, a hysteresis controller that has an obligation of controlling and shaping the output current so that it matches the reference current is used. **Figure 5.12** presents the conceptual waveforms of the sinusoidal hysteresis controller.
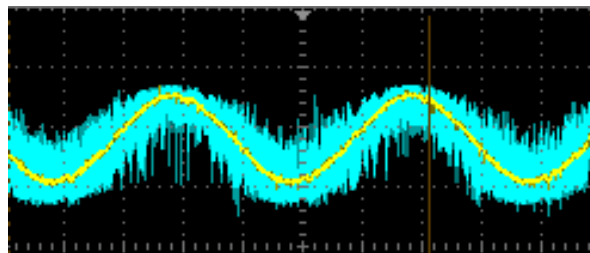
Figure 5.12 Conceptual waveforms of the sinusoidal hysteresis controller

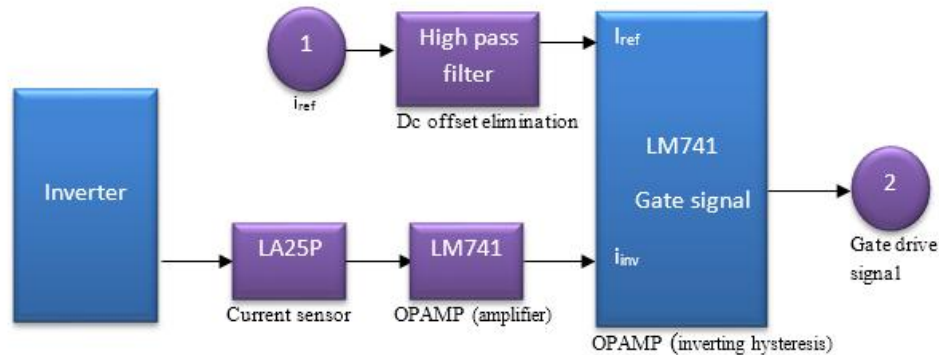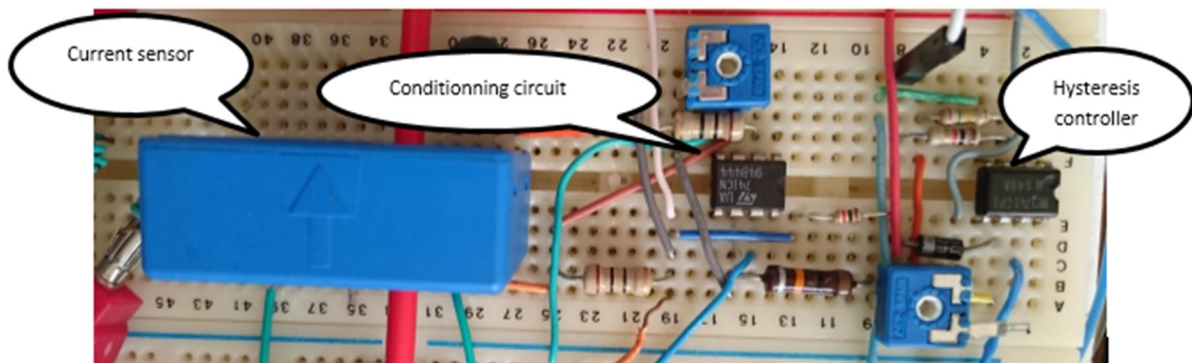According to **figure 5.12**, the controller receives two inputs, the reference current generated from the microcontroller multiplied by the MPPT's output signal, and the feedback current from the inverter's output, the system's block diagram is shown in **figure 5.13**. While its actual circuit is shown in **figure 5.14.**

Figure 5.13 Hysteresis controller block diagram

Figure 5.14 Hysteresis controller's circuit

6.1-   Inverter's current sensor

The same Hall Effect current sensor and its signal conditioning circuit are used for AC current measurement, as shown in **figure 5.14**.

6.2-   Hysteresis controller using Schmitt trigger

Schmitt trigger is a comparator circuit with hysteresis. It is implemented by applying positive feedback to the noninverting input of the comparator. It is an active circuit that converts an analog input signal to a digital output signal. The circuit is named a "trigger" because the output retains its value until the input changes sufficiently to trigger a change. In the non-inverting configuration:

$$output = \begin{cases} high, & \text{when the input is higher than a chosen threshold} \\ low, & \text{When the input is below a different (lower) chosen threshold} \\ \text{retain previous value,} & \text{when the input is between the two levels} \end{cases}$$

Schmitt trigger circuit using opamp is shown in **figure 5.15**.
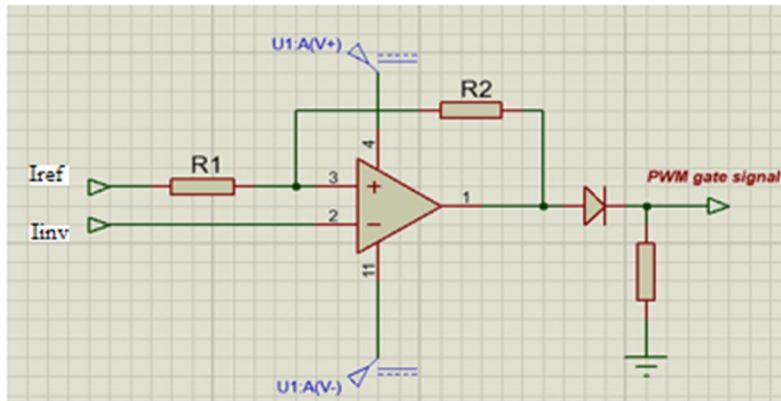
Figure 5.15 Non Inverting Schmitt trigger

The hysteresis band is given by:

$$H = \frac{R_1}{R_1+R_2}\,(V_H\text{-}V_L) = 2V_{CC}\,\frac{R_1}{R_1+R_2} \tag{5.3}$$

The hysteresis band can be adjusted to 10% of the output current amplitude by fixing the resistance R1 and use a variable resistance in the feedback loop.

❖ The resistor values for the hysteresis circuit are dependent on the output current signal.

The circuit is implemented using LM741 IC, as illustrated in **figure 5.14**.

7- GCPV system implementation

After building and testing all the circuits, the system, **figure 5.16**, is built and tested for different periods during the day.


Figure 5.16 GCPV system implementation

8- Discussion &results

> ➢ In order to validate and tune the proposed control system, a DC power supply has been used. Then, it has been changed with a SUNTECH panel (50W at STC).

> ➢ The implementation of Grid connected PV system requires very high quality components especially in their dynamic characteristics, using the available resources in the institute to implement the system has proved that this is feasible.

> ➢ The obtained results are shown in the following figures.

First, the inverter was implemented and tested, dead time, gate signals and output are shown in **figure 5.17**:

| (a) | (b) | (c) |
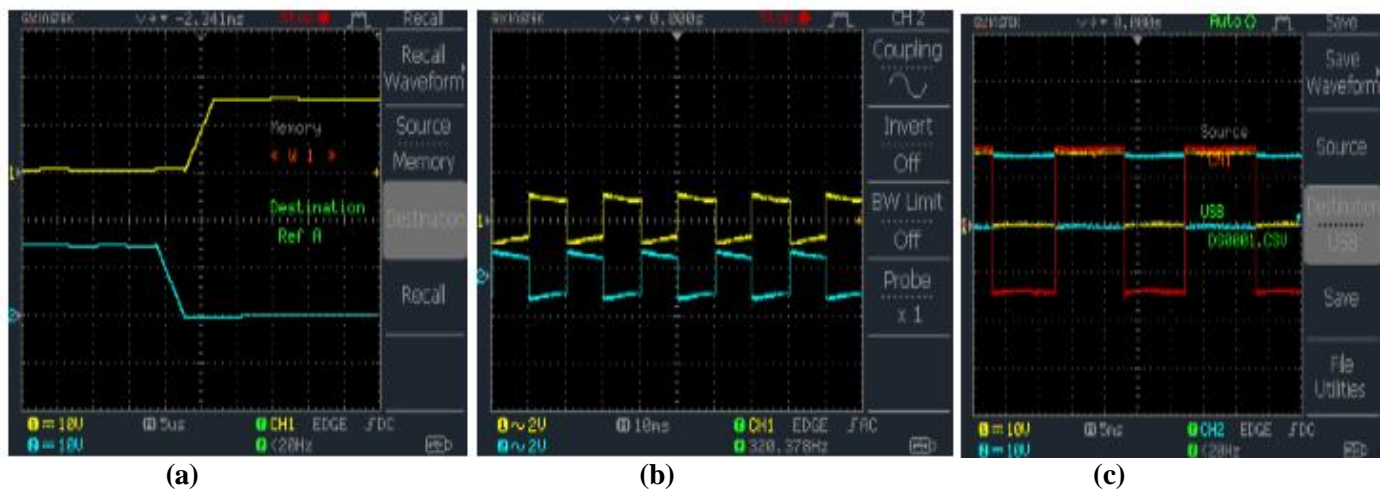
Figure 5.17 DC to AC inverter's **(a)** Dead time. **(b)** Gate signals. **(c)** Output

Once the inverter is validated. The hysteresis control system is connected , the resulting output current is close to the one in the simulation; it is out of phase with 180 degrees compared with the grid voltage (current flows from the inverter to the grid), and it kept following the generated reference signal .

The inverter's output current vs the reference current is shown in **figure 5.18.**
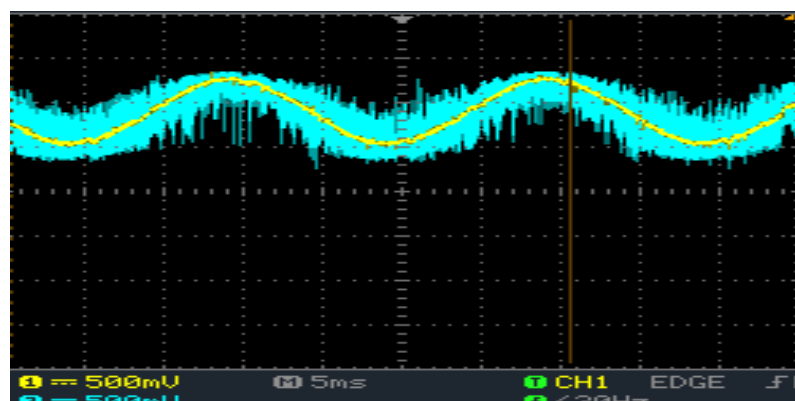
Figure 5.18 Inverter's output current VS reference current

The inverter's gate signals, output voltage (before filtering) and output current VS grid voltage are shown in **figures 5.19, 5.20, 5.21** respectively.
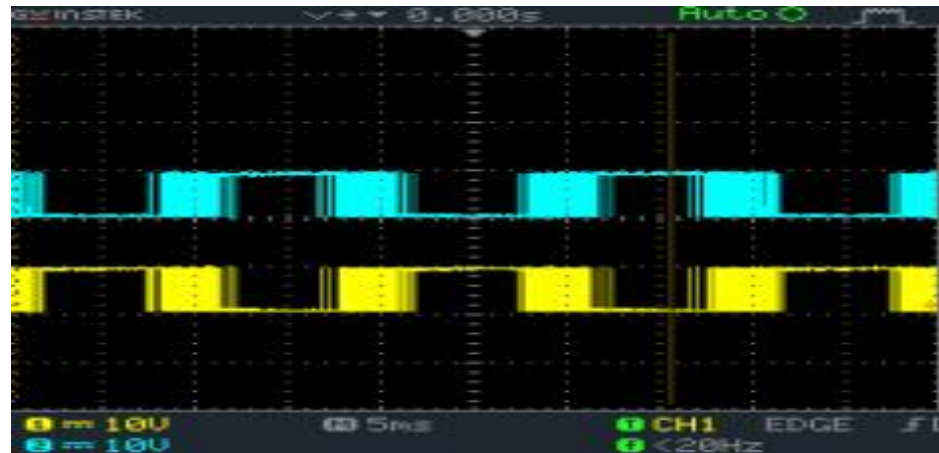
**Figure 5.19** Inverter's gate signals

Figure 5.20 Inverter's output voltage (before filtering)
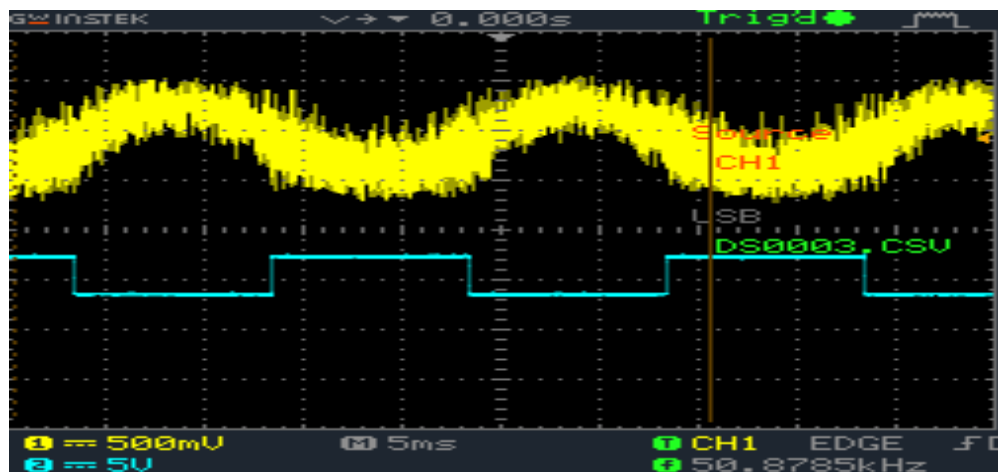
**Figure 5.21** Inverter's output current VS grid voltage

➢ After obtaining the current using DC power supply, it has been replaced by the available panel (SUNTECH STP050D 12MEA).

➢ The output of PV model is not constant and it is too small. So in order to maximize it the MPPT program has been executed. The current starts with very low value corresponding to 0.1 initial duty cycle and increases until it reaches the maximum power where it stabilizes, **figure 5.22** shows the obtained results using the PV panel.
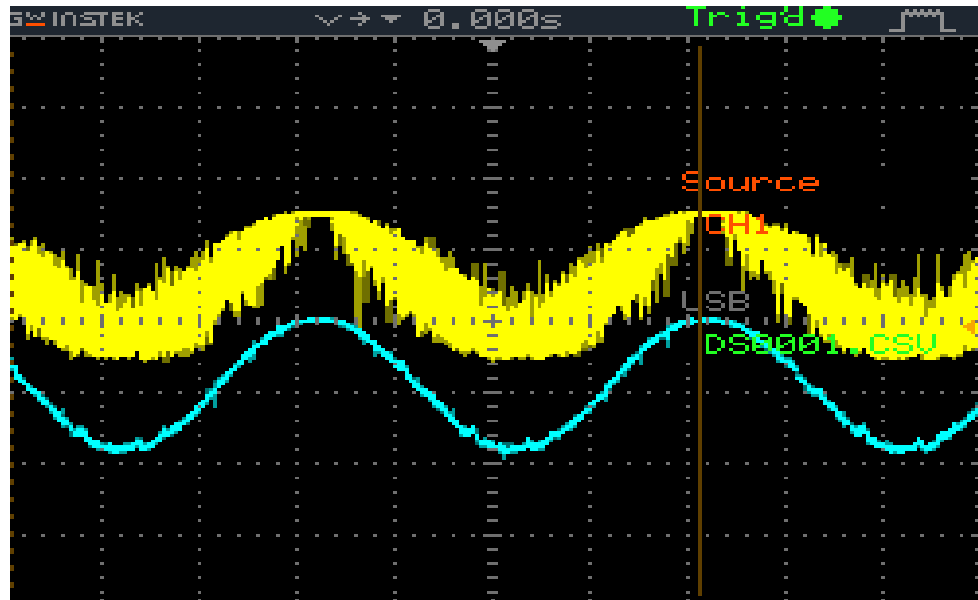
Figure 5.22 Inverter's output current using PV panel

➢ As it was expected the control system forced the output current to follow the reference current to be 180 degrees out of phase with the grid voltage.

➢ Using a power resistance of 25W and at maximum power point: V = 19.78V and I = 0.95 A so the output power reached 18.79 W. (T = 19°C; G = 500 W/m$_2$) cloudy day.

➢ After choosing suitable values of the L C filter, the system will finally be ready to be interconnected with the grid and it is highly recommended to design a protection system against all the abnormal conditions and the faults which can damage the whole system.

➢ Using a step up transformer and LabVolt power supply, the grid injection is performed and the injected current is shown in **figure 5.23.**

➢ Under the same whether conditions the injection test resulted in 0.45A AC current.
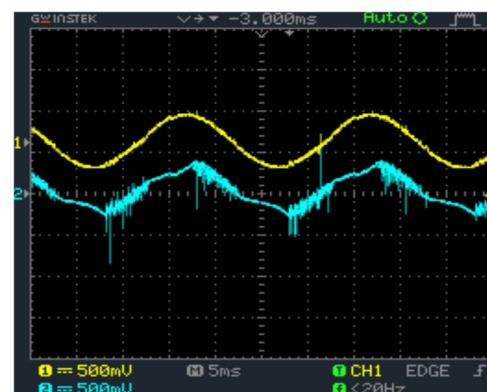
Figure 5.23 The injected current

9-   Conclusion

- In this chapter the whole system was implemented and tested.
- The obtained results showed that the Hysteresis current controller is feasible and it provides good results in terms of control of injected current
- The irradiance was very low the day when the tests was performed which explains the low output power of the panel.
- The inverter's output voltage must be filtered and stepped up to match the grid requirement, it can be concluded also that the hysteresis controller allows to simplify the system architecture. In other words, the chopper stage has been removed.

1-   Conclusion

The presented work dealt with the analysis, design, simulation and implementation of a single-phase, single-stage, Grid-Connected Photovoltaic System (GCPV), using Hysteresis Current Control Inverter. The goal of our work was to extract the maximum power from the panel, convert it to AC power then inject it into the utility grid.

Before designing our system, several factors were taken into consideration: signals synchronization, minimization of THD, speed of response, maximum power extraction and design complexity. In this regard, the controller combines the hardware speed and software compatibility.

While stepping through the simulation and implementation processes, three variables were isolated, measured and sent to the processor (the Arduino microcontroller for implementation and matlab for simulation), these variables are PV voltage (V_{pv}), PV current (I_{pv}), for maximum power point tracking, and grid voltage (V_{grid}), for the output current synchronization.

At the beginning of the process, a rectified sinusoidal waveform (I_{sine}) is generated from V_{grid}, the maximum power point of the PV panel is simultaneously tracked from V_{pv} and I_{pv} by controlling the output current so that $dP/dV = 0$. At the maximum power point, an optimum current is calculated and a reference current (I_{ref}) is generated by scaling I_{sine} with the optimum current. Hysteresis controller is then used in order to shape the inverter current I_o to match I_{ref}.

As a result, the output current had exactly the same frequency as the grid voltage; the amplitude of I_o is varied to match the maximum power provided by the photovoltaic. In the system implementation the processor is programmed to stop all process whenever the grid goes offline.

The simulation of the system provided high performance characteristics from the MPPT tracking in the DC side to the low THD (The grid interconnection of a PV power generation system must respect the IEEE-1547 interconnection standard, which requires a THD less than 5%. In this simulation an acceptable THD of (4.84 %) has been reached), and controller reliability in the AC side, also, the system showed a remarkable robustness against weather variations.

Wherein for the implementation this power system was tested during noon until 4 P.M. of May, 19th, 2016. The system was connected with 50-W photovoltaic panel which was installed in the opened space where it could be reached by sunlight. The performance of the system was calculated and set in this report.

It must be mentioned that, the panel used in the simulation was a 240W; however, in the implementation only one module of 50W was available, and due to the system losses and security issues, it was very difficult to inject current in the grid. However we have successfully tested our hysteresis current controller and the whole system worked as expected.

This proposed configuration can greatly reduce the existing power demand, limits the use of conventional power generation techniques, and also it is the only mean to tackle the future power requirement. It saves the fossil fuels from depletion, limits global warming and keeps the environment clean and green, if many PV arrays are employed.

2-   **Further work:**

There are possible directions to work on the way to improve further system performance, design simplicity and flexibility.

The MPPT method used in this system can be replaced with other methods and a better efficient tracking can be obtained. The various current control methods and DC voltage controllers can be investigated to improve the quality of the injected current. Also a fault detection and protection system may be suggested in addition to monitoring system in the case of large power plants in order to improve the system reliability.

References

[1]   Z. Sen, (2004), "Solar energy in progress and future research trends." *Progress in Energy and Combustion Science,* 30, pp. 367-416, 2015.

[2]   A. Benzekri, "FPGA-Based intelligent dual-axis solar tracking control system", *2015* pp. 19.

[3]   P. Fornasiero, M. Graziani, (2006), Renewable *Resources and Renewable Energy: A Global Challenge*, 2nd Edition, Taylor & Francis, 2015.

[4]   H. Scheer,(2004), The Solar Economy: Renewable Energy for a Sustainable Global Future, Earthscan, 2015.

[5]   "Planning and installing photovoltaic systems", (2008): a guide for installers, architects, and engineers / Deutsche Gesellschaft fur Sonnenenergie (DGS). - 2nd ed.

[6]   florida solar energy center (2007-2014) history of PV, http://www.fsec.ucf.edu/en/consumer/solar_electricity/basics/history_of_pv.html april, 2015

[7]   J.A. Ramos, I. Zamora, J.J. Campayo. (March 2010) "Modeling of Photovoltaic Module", International Conference on Renewable Energies and Power Quality (ICREPQ'10) Granada, Spain, 23-25. 2015.

[8]   Paula Mints Founder/Chief Market Research Analyst (August 21, 2013) Off-grid Solar Applications, Where Grid Parity Is Truly Meaningless http://www.renewableenergyworld.com / articles/2013/08/off-grid-solar applications-where-grid-parity-is-truly-meaningless.html, 2015.

[9]   Miro Zeman Delft University of Technology, Chapter 9. Photovoltaic systems, SOLAR CELLS.

[10]   The National Energy Foundation, The National Energy Centre,(2008), types of photovoltaic (PV) cells. http://www.nef.org.uk/knowledge-hub/solar-energy/types-of-photovoltaic-pv-cells), january,2015.

[11]   Detlef Schulz, Matthias Jahn and Thomas Pfeifer, 'Grid Integration of Photovoltaic and Fuel Cells', Power Electronics in Smart Electrical Energy Networks Power Systems Page375-407.

[12]   pure energies group, Inc (2014),types of solar apnels, http://pureenergies.com/us/how-solar-works/types-of-solar-panels, January,2015

[13]   Chenming Hu and Richard M. White (1983),SOLAR CELLS From Basics to Advanced Systems, Stephen W. Director, Carnegie-Mellon University, University of California, Berkeley

[14]   sunstation Scotland (2011), How it works, http://www.sunstationscotland.net, march, 2015

[15]   alternative energy solutions for the 21st century, http://www.altenergy.org/renewables/solar/common-types-of-solar-cells.html, March, 2015

[16]   florida solar energy center (2007-2014) how PV cells work, http://www.fsec.ucf.edu/en/consumer/solar_electricity/basics/how_pv_cells_work.htm, April, 2015.

[17]   Today Business newspaper, TYPES OF PHOTOVOLTAIC SYSTEMS, P 10, Monday 28 May, 2012.

[18]   florida solar energy center (2007-2014) types of PV systems, http://www.fsec.ucf.edu/en/consumer/solar_electricity/basics/types_of_pv.htm, april,2015

[19]   Habbati Bellia, Ramdani Youcef, Moulay Fatima (2014), A detailed modeling of photovoltaic module using MATLAB, NRIAG Journal of Astronomy and Geophysics Volume 3, Issue 1, June 2014, Pages 53–61.

[20]   Ram Naresh Bharti, Rajib Kumar Mandal, (July - 2014) Modeling and Simulation of Maximum Power Point Tracking for Solar PV System using Perturb and Observe Algorithm International Journal of Engineering Research & Technology, Vol. 3 - Issue 7.

[21]   Euzeli cipriano dos santos Jr, Edison Roberto Cabral da Silva (January 2015) advanced power electronics converters PWM converters processing AC voltage.

[22]   Paul F. Fillmore (March 16, 2012) design, construction, and testing of a hysteresis controlled inverter for paralleling.

[23]   B.Venkata Ranganadh, A. Mallikarjuna Prasad, Madichetty Sreedhar (September 2013) Modelling And Simulation Of A Hysteresis Band Pulse Width Modulated Current Controller Applied To A Three Phase Voltage Source Inverter By Using Mat lab, vol 2, issue 9.

[26]   IEEE Std 519-1992, (April 9 1993), IEEE Recommended Practices and Requirements for Harmonic Control in Electrical Power Systems, New York, NY: IEEE

[27]   E-Habrouk M., Darwish M.K., Mehta P., (2000), "Active power filters: a review", IE Proceedings-Electric Power Applications, Vol. 147, Iss. 5, pp. 403-413.

[28]   Akagi H., (2005) "Active harmonic filters", Proceedings of the IEEE, Vol. 93, Iss. 12, pp. 2128-2141.

[29]   Marco Liserre, Frede Blaabjerg, Steffan Hansen, (2005) "Design and Control of an LCLFilter-Based Three-Phase Active Rectifier", IEEE Transactions on Industry Application, Vol. 41, No. 5, pp. 1281-1291.

[30]   Rammar, (Nov 25, 2015), EITEN AUS 03 FILTERSCHALTUNGEN GB 130 134.

[31]   https://en.wikipedia.org/wiki/Gate_driver